Contrib Mineral Petrol (2003) 145: 550–567
DOI 10.1007/s00410-003-0469-7

ORIGINAL PAPER

Daisuke Nakamura

Stability of phengite and biotite in eclogites and characteristics of biotite- or orthopyroxene-bearing eclogites

Received: 30 May 2002 / Accepted: 29 March 2003 / Published online: 28 May 2003

Abstract Stability of phengite and biotite in eclogite is discussed using petrological data of natural eclogites, and the observational data are examined by thermodynamic calculations. Generally, phengite is a major K phase in natural eclogite and is stable in wide range of bulk composition. However, in eclogites from several localities of the Caledonides, biotite occurs as a stable eclogite-facies mineral, and is often associated with orthopyroxene. Bulk compositions of such biotite- or orthopyroxene-bearing eclogites are compared with those of eclogites from the Dabie–Sulu region, China, where phengite is a major K phase in eclogite. The biotite- or orthopyroxene-bearing eclogites from the Western Gneiss Region of the Caledonides are rich in MgO (10–15 wt%) and relatively poor in CaO (7–8 wt%) and Al_2O_3 (12–16 wt%). The CaO/MgO ratios of the biotite- or orthopyroxene-bearing eclogites are clearly lower than those of eclogites from the Dabie–Sulu region, indicating that MgO-rich and CaO-poor environments should be important for stabilizing of biotite and orthopyroxene in eclogite. Biotite-bearing eclogite from the North-East Greenland Eclogite Province is rich in MgO ($\approx$ 16 wt%) and CaO ($\approx$ 15.5 wt%) and extremely poor in Al_2O_3 ($\approx$ 8 wt%). To stabilize biotite in eclogite, Al_2O_3-poor environments are also important. Bulk compositions of these biotite- or orthopyroxene-bearing eclogites are similar to picrite basaltic compositions. To examine these observational data, thermodynamic calculations were carried out in a seven-component system $KH_2O_{1.5}$–Na_2O–CaO–FeO–MgO–Al_2O_3–SiO_2, which includes garnet, kyanite, phengite, biotite, quartz, omphacite, orthopyroxene and olivine in conjunction with mass-balance calculations. Firstly, calculations were performed on the average bulk composition of eclogites from the Dabie–Sulu region to lherzolite (KLB-1). The calculation results confirmed that phengite should be stable in eclogite with 'ordinary' basaltic composition, whereas biotite and orthopyroxene should be stable in picrite basaltic compositions (e.g. MgO >11.0 wt%, CaO <9.8 wt%, Al_2O_3 <15.2 wt% at 700 °C, 2.5 GPa). Further calculations in basaltic system confirmed that increase of MgO content and decrease of CaO and Al_2O_3 contents were important to stabilize biotite and orthopyroxene in eclogite. Thus, mineral assemblage in picrite basalt system should be completely different from that in normal basaltic system.

D. Nakamura (✉)
Department of Geology and Mineralogy,
Graduate School of Science, Kyoto University,
606-8502 Kyoto, Japan
E-mail: daisuke@terra.kueps.kyoto-u.ac.jp
Tel.: +81-75-7534150
Fax: +81-75-7534189

Editorial responsibility: V. Trommsdorff

Introduction

The pressure–temperature (P–T) conditions required for the formation of eclogite are generally met in a subduction zone environment, although it can also be stable near the crust–mantle boundary in stable continental crust (e.g. Griffin et al. 1990). Hydrous minerals occur in many eclogites formed by subduction of continental or oceanic crust materials, and understanding the stability of such minerals is important for elucidating the processes of magmatism and the recycling of H_2O in the subduction zone. Recently, ultrahigh-pressure (UHP) metamorphic rocks have been reported from several orogenic belts, and they can give direct information on which hydrous minerals were present in eclogites dragged down to more than 100-km depth. Indeed, various kinds of hydrous minerals were present in UHP eclogites. Especially, phengite (Phn) is a common hydrous mineral in UHP eclogites from several orogenic belts (e.g. Kienast et al. 1991; Schmädicke

et al. 1992; Enami et al. 1993; Carswell et al. 1997) and should be an important H_2O carrier, stable up to about 300-km depth in basaltic and pelitic systems (e.g. Domanik and Holloway 1996, 2000; Schmidt 1996; Ono 1998). Phengite is commonly present also in eclogites formed by subduction of oceanic basalt (e.g. Clarke et al. 1997). Other representative hydrous phases in natural eclogite are amphibole (Amp), epidote (or zoisite) (EZ) and paragonite (Pg). On the other hand, some eclogites in the Caledonides contain stable biotite (Bt) even in basaltic composition (e.g. Jamtveit 1987a). Eclogite in this orogenic belt is also characterized by the occurrence of orthopyroxene (Opx). Thus, various kinds of mineral assemblages are observed in natural eclogites, but the relationships between bulk composition and mineral assemblage are not clear. Therefore, this study summarizes the relationships between mineral assemblage and bulk composition in natural eclogites, and especially stability relations between phengite and biotite are discussed. Furthermore, the compiled data are used to understand the reason why biotite and orthopyroxene formed in some eclogites and not others, and then the results are examined by thermodynamic calculations in a multi-component system.

Mineral assemblages of eclogite

The mineral assemblages of natural eclogites in several orogenic belts have been compiled. In this paper, 'mineral assemblage' refers to a stable assemblage at peak-P metamorphic conditions of eclogite (mineral abbreviations mainly follow Kretz 1983, and are listed in Table 1). However, formation stage of some minerals in eclogite is difficult to identify by textural information alone. For example, in the Sulu region, UHP metamorphic province in China (e.g. Ernst and Liou 1995), some eclogites contain euhedral and poikiloblastic epidote (Fig. 1A). Inclusions in such epidote are eclogite-facies minerals; garnet (Grt) + omphacite (Omp) + quartz (Qtz) and/or quartz pseudomorphs after coesite (Coe). In some cases, kyanite (Ky) also shows poikiloblastic texture (Fig. 1A). Theses poikiloblasts were probably stable at peak-P conditions (>3 GPa), but could also be decompressional products. Synthetic experiments (e.g. Poli and Schmidt 1995) have shown

Table 1 Mineral abbreviations

Phase	Abbreviation
Phengite	Phn
Amphibole	Amp
Epidote or Zoisite	EZ
Paragonite	Pg
Biotite	Bt
Orthopyroxene	Opx
Garnet	Grt
Omphacite	Omp
Quartz	Qtz
Coesite	Coe
Kyanite	Ky
Rutile	Rt
Quartz or coesite	QC
Talc	Tlc
Olivine	Ol
Augite	Aug
Pyrope	prp
Grossular	grs
Almandine	alm
Diopside	di
Phlogopite	phl
Enstatite	en
Jadeite	jd
Hedenbergite	hd
Forsterite	fo

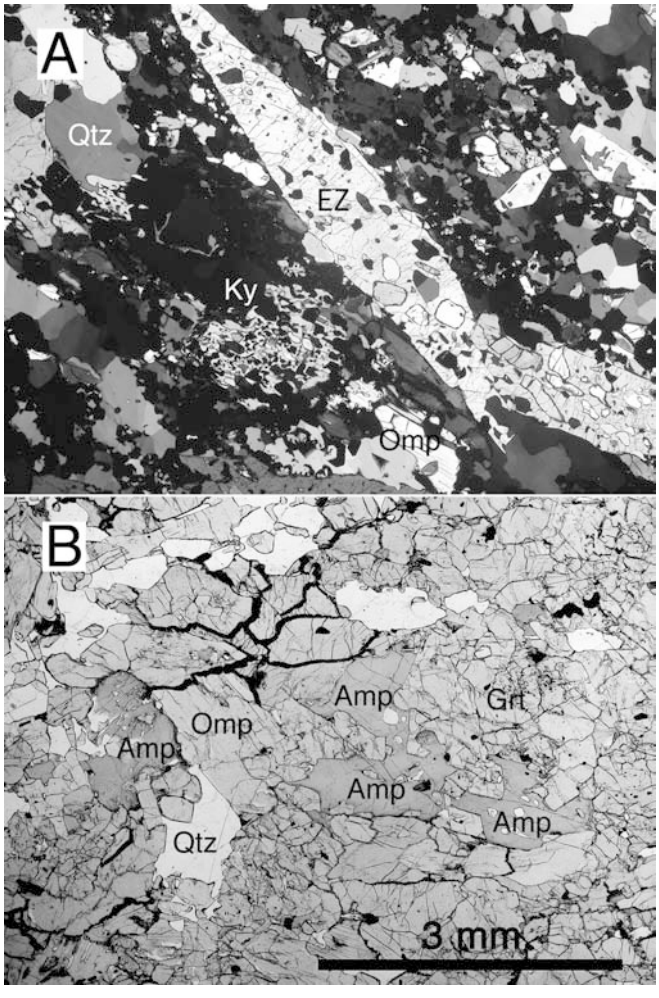

Fig. 1A, B Photomicrographs of eclogites from Donghai in the Sulu region, China. **A** Epidote (*EZ*) occurs as large euhedral grains and shows poikiloblastic texture. Kyanite (*Ky*) also shows poikiloblastic texture. *Qtz* Quartz; *Omp* omphacite. Crossed-polarized light. **B** Amphibole interstitially grows among garnet (*Grt*), omphacite and quartz. Plane polarized light

that zoisite is unstable above ≈3 GPa in basaltic composition. Pale green-to-blue amphibole is also present as relatively large grains that grew interstitially among the eclogite-facies minerals (Fig. 1B). The eclogite containing such amphibole is less overprinted by the amphibolite- or granulite-facies minerals, suggesting that it grew under the eclogite-facies conditions. According to synthetic experiments (e.g. Liu et al. 1996), amphibole is unstable at UHP conditions in the mid-ocean ridge basalt (MORB) system. However, Hirajima et al. (1992) found nyböite [$NaNa_2Mg_3Al_2Si_7Al(OH)_2$] in eclogite from the Sulu region, and in the Dora Maira massif, the western Alps, glaucophane occurs in UHP sodic white schist (e.g. Kienast et al. 1991). Such Na-rich amphibole may be stable even at UHP conditions depending on the bulk compositions. The stability of amphibole in UHP eclogite, therefore, is still debatable, and determination of the peak-P mineral assemblage is difficult. As a consequence, the mineral assemblages compiled in this study, especially the amphibole and poikiloblastic phases, may not have been stable at peak-P conditions.

The Dabie–Sulu region, eastern China, is a UHP metamorphic belt. In such orogenic belts, eclogite generally occurs as blocks (or lenses) included in country gneiss: continental crust material. The peak metamorphic conditions of eclogites from the Dabie–Sulu region were estimated to be 700–880 °C, 2.9–4.1 GPa (e.g. Carswell et al. 1997; Nakamura and Banno 1997; Hirajima and Nakamura 2003). The main constituents of eclogite are Grt, Omp, rutile (Rt) and SiO_2-phases (quartz or coesite: QC). The representative mineral assemblage of eclogites from the Dabie–Sulu region is Grt + Omp + Rt + QC accompanied by Phn, Ky, Amp or EZ (e.g. Hirajima et al. 1990; Enami et al. 1993; Okay 1995; Zhang et al. 1995a; Carswell et al. 1997; Nakamura and Hirajima 2000). The presence of K-feldspar, talc (Tlc), dolomite and aragonite has been reported in a few cases (Enami et al. 1993; Zhang et al. 1995a, 1995b; Carswell et al. 1997), and apatite and zircon are common accessory minerals (e.g. Enami et al. 1993). According to my observations of about 400 thin sections of eclogitic samples from the Sulu region, about 40% of them contain phengite as an eclogite-facies mineral (Fig. 2). Although biotite grains are also present in eclogites, they are closely associated with plagioclase and formed mainly after phengite (e.g. Fig. 3f of Enami et al. 1993); i.e. they formed under amphibolite- or granulite-facies conditions during the ascent of the eclogites. Thus, phengite is the representative K phase in the eclogite of this region. However, in Rongcheng and Weihai of the north-eastern Sulu region, phengite is very rare (Fig. 2) and occurs only as a minor inclusion in other eclogite-facies minerals. This may be due to phengite dehydration melting of eclogite during exhumation (Ye et al. 2001); phengite dehydration melting of acidic rocks probably occurred in this area (Hermann 2002).

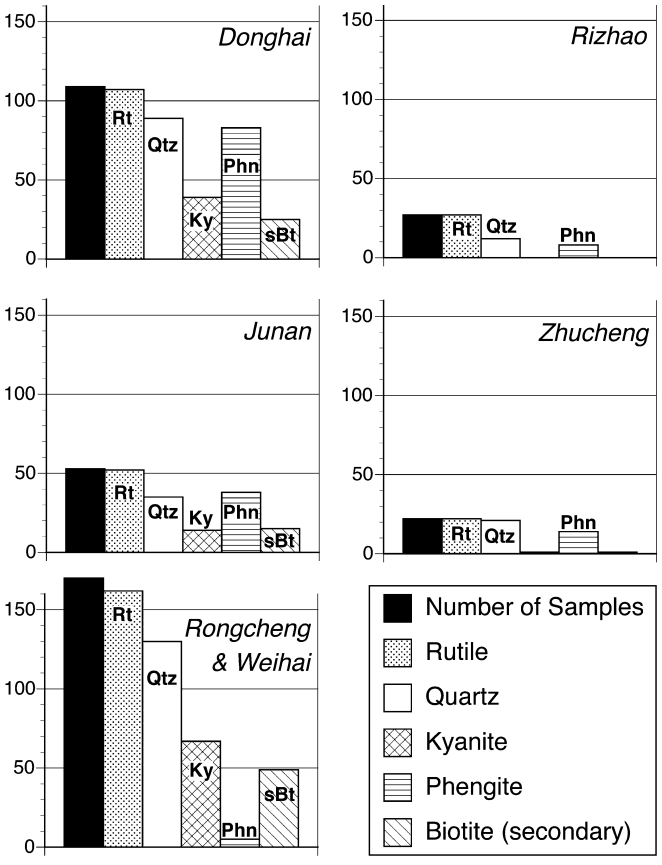

Fig. 2 Frequency of mineral occurrence in eclogitic rocks from the Sulu region. Each *black bar* represents the total number of observed samples in each area. The other *vertical bars* show the number of samples in which rutile (*Rt*), quartz (*Qtz*), kyanite (*Ky*), phengite (*Phn*) or secondary biotite (*sBt*) is present. Secondary biotite means biotite that formed in the amphibolite- or granulite-stages during the decompression of the eclogites. The other phases formed at the eclogite-facies stage

Also, in other representative orogenic belts, phengite is the major K phase in eclogite as described below. In the UHP unit of the southern Dora Maira massif, the western Alps, the typical mineral assemblage of eclogite is Grt + Omp + Rt + QC accompanied by Phn, Ky, EZ or Amp (e.g. Chopin et al. 1991; Kienast et al. 1991; Compagnoni et al. 1995). In the Qtz-stable units of the European Alps, eclogite is accompanied by Phn, Ky, Amp, EZ, Pg, Tlc or chloritoid (e.g. Holland 1979; Heinrich 1982, 1986; Droop et al. 1990). In the Saxothuringian zone of the Variscides, eclogites are accompanied by Phn, Ky, Amp or EZ (e.g. O'Brien et al. 1990; Okrusch et al. 1991; Schmädicke et al. 1992; O'Brien 1993), although the presence of biotite has been reported in an eclogite from the central Erzgebirge (Schmädicke et al. 1992). Eclogite-stage biotite has been reported from an eclogite sample in the Moldanubian zone of the Variscides (Medaris et al. 1995). In north-eastern New Caledonia, eclogite occurs in a high-grade zone, and the mineral assemblage of the eclogite is Grt +

Table 2 Mineral assemblages of eclogites from the Dabie–Sulu region and the Caledonides. *Grt* Garnet; *Omp* omphacite; *Rt* rutile; *QC* quartz or coesite; *Phn* phengite; *Bt* biotite; *Kfs* K-feldspar; *Ky* kyanite; *Opx* orthopyroxene; *Amp* amphibole; *EZ* epidote or zoisite. + Present; ± present in some samples. *NEGEP* North-East Greenland Eclogite Province

Suture zone	Mineral assemblages												
Area	Grt	Omp	Rt	QC	Phn	Bt	Kfs	Ky	Opx	Amp	EZ	P–T conditions	Reference
Dabie–Sulu region													
Bixiling (BXL4)	+	+		+	+	+			+			700–880 °C, 2.9–4.1 GPa	This study
Qinglongshan (QL1)	+	+		+	+	+			+		+	700–880 °C, 2.9–4.1 GPa	This study
Yangkou (YK34a)	+	+		+	+	+			+		+	700–880 °C, 2.9–4.1 GPa	This study
Caledonides													
Nordfjord-Stadlandet	+	+		+	+	+			±		±	750–850 °C, 2.7–3.0 GPa	Wain et al. (2000)
	+	+		+	+	±	+			±		750–850 °C, 2.7–3.0 GPa	
(Selje)	+	+		±	±		±			±		700–850 °C, 3.0–4.3 GPa	Lappin and Smith (1978)
Hareidlandet	+	+		+	±		±			±		≈ 750 °C, > 2.0 GPa	Jamtveit (1987a)
	+	+		+	+	±		+				≈ 750 °C, > 2.0 GPa	
Flemøy	+	+		±	±		±			±		≈ 750 °C, > 2.0 GPa	Mørk (1985)
Kristiansund	+	+		+	+		+					≈ 750 °C, ≈1.85 GPa	Krogh (1980)
NEGEP	+	+		±	±	±	±			±		700–800 °C, 1.5–2.4 GPa	Brueckner et al. (1998)
	+	+		±	±			±		±	±	700–800 °C, 1.5–2.4 GPa	

Omp + EZ + glaucophane + barroisite ± Phn ± Qtz ± Pg (e.g. Brothers and Yokoyama 1982; Clarke et al. 1997).

In contrast to the above examples, in the Caledonides of the Western Gneiss Region (WGR), Norway, and the North-East Greenland Eclogite Province (NEGEP; Brueckner et al. 1998), Bt-bearing eclogites occur in several localities (Table 2). Widespread occurrence of coesite and its pseudomorphs in eclogite has been reported from the Nordfjord and Stadtlandet area of the WGR (Smith 1984, 1988; Wain 1997; Wain et al. 2000; Cuthbert et al. 2000). The estimated P–T conditions of this UHP area are 700–850 °C, 2.7–4.3 GPa (Lappin and Smith 1978; Wain 1997; Cuthbert et al. 2000). Common assemblage of the UHP eclogite is Grt + Omp + QC + Rt accompanied by Phn, Ky, EZ or Amp, but at a few localities biotite occurs in Mg-rich and Ky-free eclogites (Wain et al. 2000; Table 1), suggesting that bulk composition is an important factor for the formation of eclogite-facies biotite. In this area, orthopyroxene often occurs in eclogites (e.g. Lappin and Smith 1978; Smith 1984). Also, in other localities of the WGR, such as Kristiansund, Flemsøy and Hareidlandet, biotite and orthopyroxene occur in eclogites (Krogh 1980; Mørk 1985; Jamtveit 1987a). For these localities, metamorphic P–T conditions were estimated to be ≈750 °C, 2.0 GPa by geothermobarometry, but coesite or its pseudomorphs were found around Flemsøy and Hareidlandet (see Cuthbert et al. 2000). Kyanite is absent from these Bt- or Opx-bearing eclogites (Table 2). In the review of Norwegian eclogite by Smith (1988), he showed the distinction between Ky-eclogite lineage and Opx-eclogite lineage samples. The Ky-eclogite lineage samples are associated with phengite, whereas the Opx-eclogite lineage samples are associated with biotite. The associations of Ky + Bt and Ky + Opx are probably unstable in 'ordinary' eclogitic rocks. The presence of biotite has been reported also in eclogite from the NEGEP, and eclogite-stage temperatures of this area are estimated to be 700–780 °C at P > 1.5 GPa (Brueckner et al. 1998), which is nearly the same as the values for the above Bt- or Opx-bearing localities in the WGR (Table 2). The Bt- or Opx-bearing localities are situated along the western coast of Norway in the highest-grade part of the WGR [$(Fe^{2+}/Mg)^{Grt}/(Fe^{2+}/Mg)^{Cpx}$: $K_D \leq 5$; Krogh 1977]. On the other hand, eclogites from the lower-grade part of the WGR ($K_D > 5$) mainly have the assemblages Grt + Omp + Rt ± Qtz accompanied by Phn, Pg, Amp, Ky or ZE (Krogh 1977). Biotite has not been reported in the lower-grade part by Krogh (1977); hence, high-T conditions could also be a factor for the formation of biotite in eclogite, whereas Opx-bearing eclogites are fairly common also in the lower-grade part of the WGR (Krogh 1977).

Bulk composition

As described above, Bt-bearing eclogites occur in the high-grade part of the Caledonides, whereas Phn-bearing eclogite is predominant in the other orogenic belts. To examine the effect of bulk composition on the occurrence of biotite in eclogite, bulk compositional data from the Caledonides and the Dabie–Sulu region were compiled (Fig. 3), and three eclogites from the Dabie–Sulu region were newly analysed (Table 3); mineral assemblages are shown in Table 2. Data from the Caledonides excludes both garnet websterite and retrograded eclogite, referred to as group Ib eclogite by Jamtveit (1987b).

Bt- or Opx-bearing eclogites from the Caledonides (Mørk 1985; Jamtveit 1987b; Brueckner et al. 1998) are

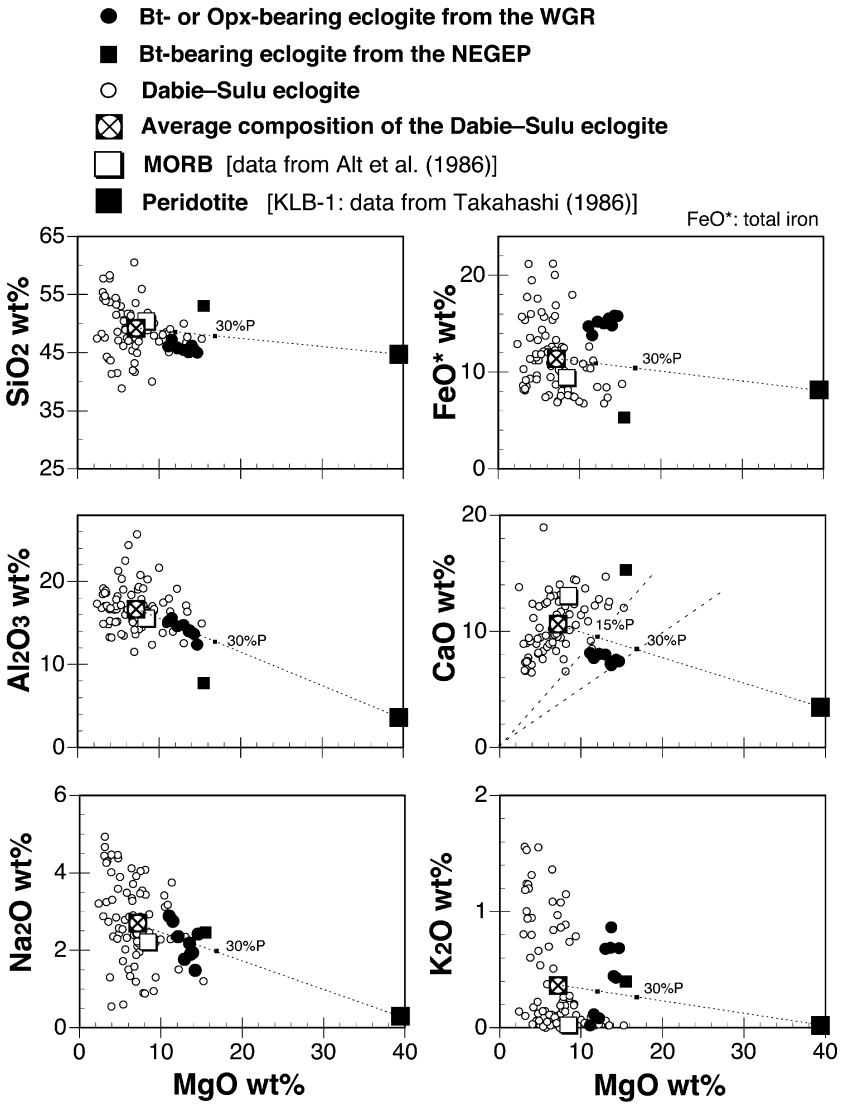

Fig. 3 Compilation of bulk compositions of eclogites from the Dabie–Sulu region (Li et al. 1993; Ye and Cong 1994; Zhang et al. 1994, 1995a, 1995b; Chavagnac and Jahn 1996; Jahn 1998). For comparison, bulk compositions of biotite (*Bt*)- or orthopyroxene (*Opx*)-bearing eclogites from the Western Gneiss Region (*WGR*) (Jamtveit 1987b) and Bt-bearing eclogite from the North-East Greenland Eclogite Province (NEGEP; Brueckner et al. 1998) are also plotted. The compositions of mid-ocean ridge basalt (*MORB*) and the peridotite (*KLB-1*) are plotted for reference. The average bulk composition of the Dabie–Sulu eclogites is similar to the MORB composition, although they are not MORB origin (Jahn 1998). Bt- or Opx-bearing eclogites from the Western Gneiss Region have clearly lower CaO/MgO ratio than the Dabie–Sulu eclogites, and they contain 15 to 30% peridotite component by weight. *15%P* 15% peridotite (KLB-1) + 85% average composition of the Dabie–Sulu eclogites. *30%P* 30% peridotite + 70% average eclogite. The Bt-bearing eclogite from the NEGEP shows extremely low Al_2O_3 content

richer in MgO than most eclogites from the Dabie–Sulu region (Li et al. 1993; Ye and Cong 1994; Zhang et al. 1994, 1995a, 1995b; Chavagnac and Jahn 1996; Jahn 1998; Fig. 3). This is also described by Smith (1988) and Wain et al. (2000); i.e. biotite occurs in Mg-rich eclogites in the WGR. The geochemical and isotopic data indicate that most of the Dabie–Sulu eclogite protoliths resemble basalts/gabbros and their metamorphic equivalents of Precambrian gneiss terranes (Jahn 1998). The average bulk composition of the Dabie–Sulu eclogite (Table 3) is shown in Fig. 3. This average bulk composition will be used as a representative eclogite in the later thermodynamic calculations, and is termed Av. eclogite in this study. On the other hand, the WGR eclogites are relatively rich in the 'peridotite component' up to about 30 wt%, compared with the Av. eclogite (Fig. 3). Thus, Bt- or Opx-bearing eclogites from the WGR are similar to picrite basalt in bulk composition. The peridotite arbitrarily used for reference is the undepleted lherzolite xenolith (KLB-1) from the Kilborne Hole crater, New Mexico (Takahashi 1986). This peridotite composition (KLB-1) will also be used in the later thermodynamic calculations, and is referred to as the 'peridotite component' against the Av. eclogite.

The ratio of CaO to MgO is useful to recognize the compositional difference between the Dabie–Sulu eclogite and Bt- or Opx-bearing eclogite from the WGR. The ratio of CaO to MgO (weight percent) of Bt- or Opx-bearing eclogites from the WGR is clearly lower (0.51–0.73) than that of the Dabie–Sulu eclogites (≥ 0.75; average $= 1.48$; Fig. 3). A mixture of 85 wt% Av. eclogite + 15 wt% peridotite has a CaO/MgO ratio of 0.79, and broadly corresponds to the boundary between the compositional ranges of the WGR and Dabie–Sulu eclogites (Fig. 3). Using this scheme (CaO/MgO ratio), Bt- or Opx-bearing eclogites from the WGR can be expressed as a mixture of

Table 3 Bulk compositions. Total iron is expressed as FeO

	BXL4[a]	QL1[b]	YK34a[c]	Av.[d]	KLB-1[e]
SiO_2	46.68	46.09	50.88	49.47	44.79
TiO_2	0.36	1.05	1.57	1.40	0.16
Al_2O_3	21.55	19.00	16.49	16.74	3.62
FeO	7.68	12.40	10.35	11.43	8.16
MnO	0.12	0.15	0.16	–	–
MgO	9.93	7.36	6.35	7.21	39.49
CaO	11.35	9.29	8.72	10.67	3.46
Na_2O	2.27	2.82	3.29	2.72	0.30
K_2O	0.07	1.06	1.34	0.37	0.02
P_2O_5	0.30	0.30	0.30	–	–
Total	100.31	99.52	99.45	100.00[f]	100.00[f]

[a]*BXL4* Kyanite- and phengite-bearing eclogite from Bixiling, Dabieshan
[b]*QL1* Kyanite- and phengite-bearing eclogite from Qinglongshan, Sulu region
[c]*YK34a* Phengite-bearing eclogite from Yangkou, Sulu region
[d]*Av.* Average composition of the Dabie–Sulu eclogite for the model calculation
[e]*KLB-1* Peridotite composition normalized for the model calculation (undepleted spinel lherzolite in New Mexico)
[f]Total wt% is normalized to 100.00, and MnO and P_2O_5 are ignored in the model calculation

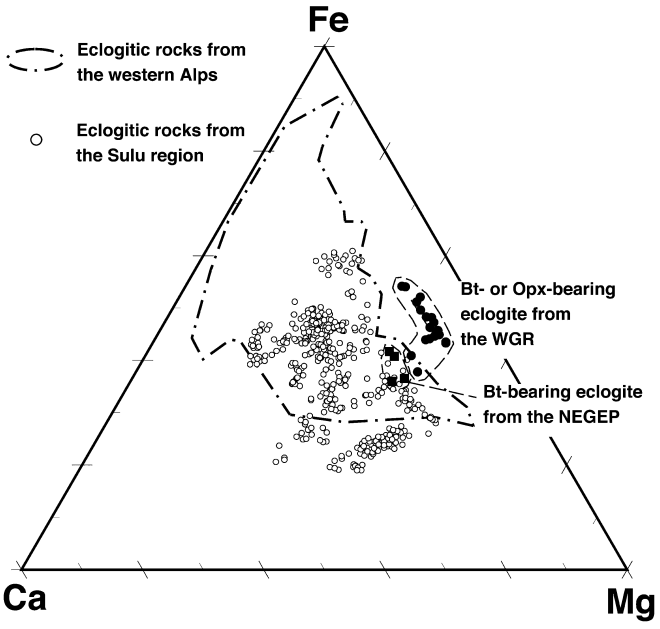

Fig. 4 Garnet compositions of eclogitic rocks from the Sulu region and of Bt- or Opx-bearing eclogites from the Caledonides. *Abbreviations* are the same as in Fig. 3. The compiled data from the western Alps (Droop et al. 1990) are also shown in this figure. Garnet of the Bt- or Opx-bearing Caledonian eclogites is poorer in the grossular component than most of the Sulu eclogitic rocks

15–30 wt% peridotite with the Av. eclogite (Fig. 3). Mg-rich and Ca-poor environments are important factors in stabilizing biotite and orthopyroxene in eclogite. Eclogite from the NEGEP also has a relatively low CaO/MgO ratio (≈1.0), but overlaps with the range shown by the Dabie–Sulu eclogites (Fig. 3). Extremely low Al content of the NEGEP eclogite probably relates to the stabilization of biotite. The Si content of the Bt-bearing eclogite from the NEGEP is relatively high (53 wt%) and, hence, low-Si content is not an essential factor for stabilizing biotite in eclogite.

Data for the Dabie–Sulu region are scattered over wide range of bulk composition (Fig. 3), indicating that phengite is stable over wide range of bulk composition, although the plotted data include phengite-free eclogites. Phengite is present even in eclogite with low K_2O contents (≈0.10 wt%), and K_2O content in omphacite should be negligible even at UHP conditions. Phengite, however, is absent from some eclogites with slightly high K_2O content (up to 0.22 wt%), and they contain amphibole (barroisite). In such amphibole-bearing eclogites, K_2O is mainly fractionated into amphibole and, hence, phengite does not occur. However, bulk compositions of amphibole-bearing eclogites have no characteristic difference compared with those of amphibole-free eclogites (e.g. Amp-bearing eclogite sample 89Q2: SiO_2 = 53.74, TiO_2 = 1.28, Al_2O_3 = 14.92, Fe_2O_3 = 4.65, FeO = 7.52, MnO = 0.22, MgO = 4.59, CaO = 9.24, Na_2O = 2.27, K_2O = 0.22 by wt%; Zhang et al. 1995a). Although it is not clear why amphibole was stabilized in some eclogites, oxygen-fugacity environments may relate to the stabilization of amphibole. Amp-bearing eclogites from Donghai in the Sulu region are often accompanied by epidote and not by zoisite. According to data by Zhang et al. (1995a), epidote-bearing eclogites have clearly high Fe_2O_3 content (> 3.5 wt%). High oxygen-fugacity environments may stabilize epidote and amphibole even in UHP conditions. Zoisite-bearing eclogites do not have high Fe_2O_3 content (< 0.60 wt%), but show high Al_2O_3 content (e.g. 23–26 wt%; Zhang et al. 1995a). In NNO-buffered synthetic experiments using basaltic compositions with not a high Al_2O_3 content (16.75 wt%), stability of zoisite was restricted to relatively low pressure conditions (< 3 GPa; Poli and Schmidt 1995), and zoisite do not appear in QFM-buffered synthetic experiments with MORB composition (Al_2O_3 = 14.80 wt%; Liu et al. 1996). Thus, stability of zoisite would be dependent on Al_2O_3 content of bulk composition. However, high CaO content would be also important to stabilize zoisite in eclogite; zoisite is present in UHP eclogite with high CaO content (= 14.38 wt%) and not a high Al_2O_3 content (= 16.66 wt%; Zhang et al. 1995b). Zoisite in Al- and Ca-rich bulk composition is probably stable even at UHP conditions, but stability of zoisite is still debatable. Kyanite also occurs in eclogites with high Al_2O_3 content, which are often accompanied by zoisite (or epidote). For eclogites from the Caledonides, kyanite-bearing eclogites can be accompanied by zoisite (or epidote; Table 2). On the other hand, Bt- or Opx-bearing eclogites are low in Al_2O_3 content (< 16 wt%), and they are not accompanied by kyanite and zoisite (or epidote).

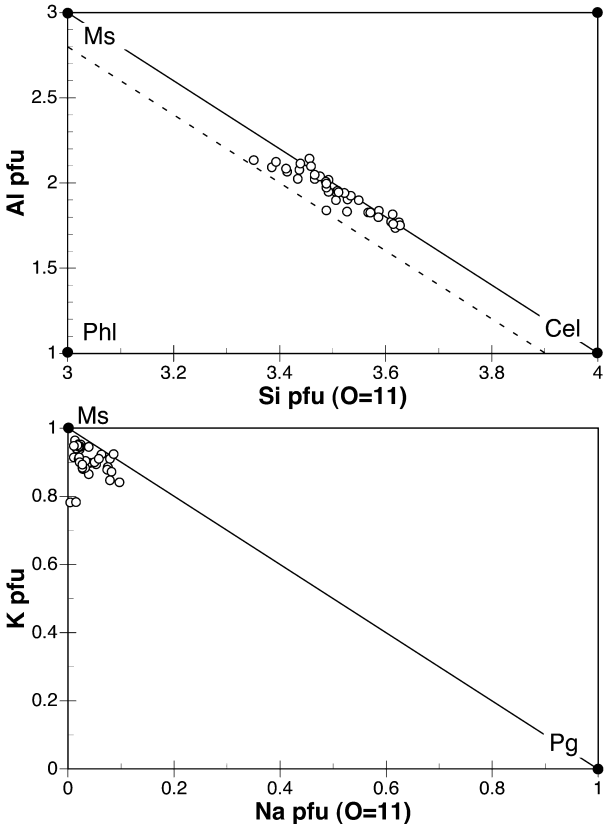

Fig. 5 Phengite compositions in eclogites from the Dabie–Sulu region, China. The *upper diagram* shows the relation between Al and Si contents (per 11 oxygens formula unit) of phengite, and the *solid line* represents ideal formula between muscovite (*Ms*) and celadonite (*Cel*). The *broken line* represents 10 mol% shift toward phlogopite (Phl) component, when Fe_2O_3 and TiO_2 are free from phengite. Phengite compositions from the Dabie–Sulu eclogites are mostly plotted along the ideal line between muscovite and celadonite. The Si content of phengite ranges from $\approx$ 3.4 to 3.6 pfu. The *bottom diagram* is plots of cation contents of K versus Na, and the *solid line* is ideal formula from muscovite to paragonite (*Pg*). Small amount of paragonite component is present in phengite from the Dabie–Sulu eclogites, and small amount of vacancy is also present in 12-fold coordinated position

Mineralogy

Garnet compositions reflect the difference in the bulk CaO/MgO ratio between Bt- or Opx-bearing eclogites from the Caledonides and eclogites from the Dabie–Sulu region. Garnet in Bt- or Opx-bearing eclogites from the WGR (Lappin and Smith 1978; Krogh 1980; Mørk 1985; Jamtveit 1987a) is poorer in grossular content ($\leq$ 20 mol%) than most garnet in eclogitic rocks from the Sulu region (Nakamura 1997; Hirajima personal communication, 1998; Fig. 4). Garnet in Bt-bearing eclogite from the NEGEP (Brueckner et al. 1998) is also poor in Ca. In addition, most of the Caledonian garnet is relatively rich in pyrope content ($\geq$ 35 mol%). Thus, the composition of garnet is mainly controlled by bulk composition, although P–T conditions also affect the composition of garnet. The garnet compositions in eclogites from the western Alps (Droop et al. 1990), where phengite is the stable K phase in eclogite, are also shown in Fig. 4. The garnet compositions in the western Alps mostly overlap the compositions of the Sulu region and display Ca contents higher than nearly all the garnet in the Bt- or Opx-bearing eclogites from the Caledonides. Thus, low Ca content of garnet is a distinctive feature of the Bt- or Opx-bearing eclogites from the Caledonides.

Chemical compositions of phengite in eclogites from the Dabie–Sulu region are compiled and shown in Fig. 5 (Hirajima et al. 1990; Okay 1995; Zhang et al. 1995a; Carswell et al. 1997; Nakamura 1997; Zhang and Liou 1997; Carswell et al. 2000; Zhang et al. 2000). Phengite in UHP eclogites contains significant amount of celadonite component, and the Si content ranges from $\approx$3.4 to 3.6 pfu based on O = 11. The compiled data are mostly plotted along the line tied between muscovite and celadonite components. However, some data may contain a small amount of biotite (phlogopite to eastonite) component that is < 10% by mole (Fig. 5); presence of Fe_2O_3 and TiO_2 also affects the plotted positions on the Al versus Si diagram for phengite. Another additional component in phengite is a paragonite component, which is contained up to about 10 mol%. The K + Na content ranges from 0.9 to 1.0 pfu except for two data (Fig. 5), and small amount of vacancy is created in a 12-fold coordinated position. TiO_2 content in phengite ranges from 0.10 to 0.90 wt%, and the Ti component is less than 5 mol% (Ti = 0.005–0.045 pfu).

Biotite compositions are also compiled and shown in Fig. 6. Eclogite-facies biotite from the Caledonides (Krogh 1980; Mørk 1985; Brueckner et al. 1998) and secondary biotite in eclogitic rocks from the Sulu region (Nakamura 1997; Zhang et al. 2000) are compared. The secondary biotite from the Sulu region is associated with plagioclase and obviously grew under plagioclase-stable conditions. The eclogite-facies biotite from the Caledonides is richer in phlogopite component (Si $\approx$2.8 pfu) than nearly all the secondary biotite from the Sulu region (Fig. 6). The Si content in biotite would increase with increasing pressure, as experimentally shown by Hermann (2002), although significant amount of the eastonite (or siderophyllite) component (up to about 30% by mole) is contained even in the eclogite-facies biotite. Most of data for both regions are plotted along the line tied between the phlogopite (or annite) and eastonite (or siderophyllite) components, and the muscovite component is negligible (Fig. 6). The eclogite-facies biotite is richer in Mg/(Fe + Mg) than most of secondary biotite from the Sulu region, which reflects the Mg-rich bulk composition of the Bt-bearing eclogites. Ti content in biotite from the Caledonides is not clearly different from that in secondary biotite from the Sulu region. The Ti-biotite component, proposed by

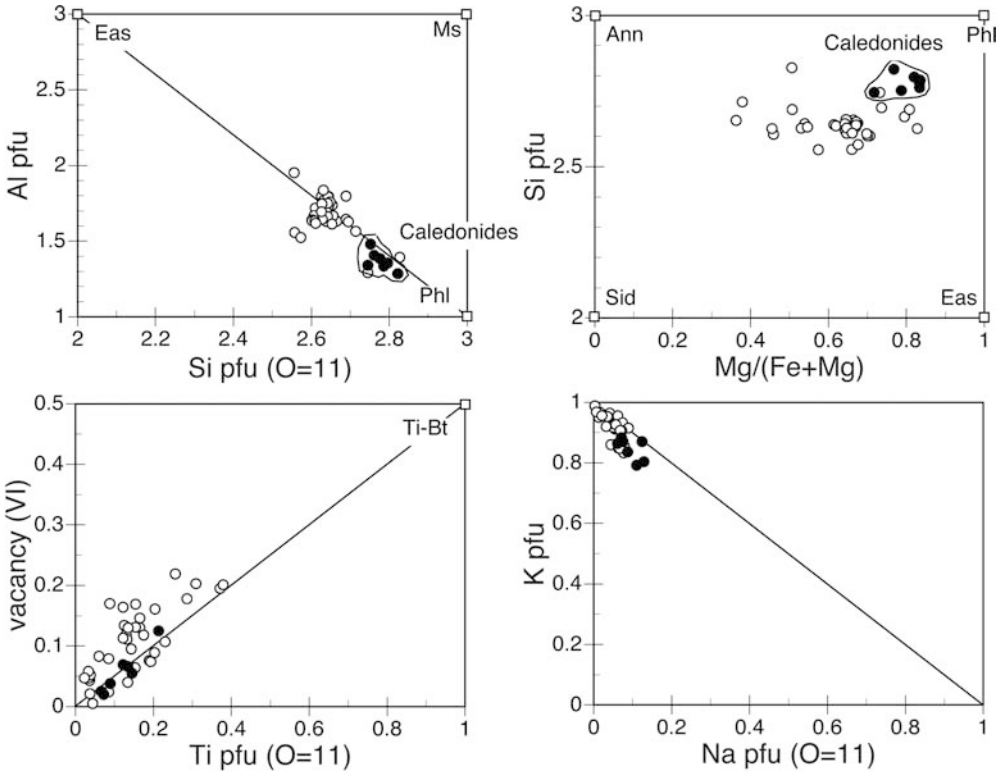

Fig. 6 Chemical compositions of biotite in eclogites from the Caledonides (*filled circle*) and in eclogitic rocks from the Sulu region, China (*open circle*). Biotite in eclogitic rocks from the Sulu region is secondary one formed under the amphibolite- or granulite-facies stages. The eclogite-facies biotite from the Caledonides is rich in the phlogopite component. Each end member is shown as *Phl* phlogopite, *Eas* eastonite, *Ms* muscovite, *Ann* annite, *Sid* siderophyllite, *Ti-Bt* Ti-biotite (Ikeda 1990). The vacancy in octahedral site is calculated as vacancy^{VI} = 7–(Si + Ti + Al + Cr + Fe + Mn + Mg) per 11 oxygens formula unit. Total iron is treated as FeO

Table 4 Assumed mineral formulae for the model calculations. A and B should be 0 to 1, and A + B should be < 1. C, D, E, F, G, H and I should be 0 to 1

Phase	Abbreviation	Formula
Garnet	Grt	$(Ca_AFe_BMg_{1-A-B})_3Al_2Si_3O_{12}$
Kyanite	Ky	Al_2SiO_5
Phengite	Phn	$K(Mg_CFe_{1-C})_DAl_{3-2D}Si_{3+D}O_{10}(OH)_2$
Biotite	Bt	$K(Mg_EFe_{1-E})_3AlSi_3O_{10}(OH)_2$
Quartz/coesite	Qtz/Coe	SiO_2
Omphacite/augite	Omp/Aug	$(Na_{1-F}Ca_F)Al_{1-F}(Mg_GFe_{1-G})_FSi_2O_6$
Orthopyroxene	Opx	$(Mg_HFe_{1-H})_2Si_2O_6$
Olivine	Ol	$(Fe_IMg_{1-I})_2SiO_4$

Ikeda (1990), is as $K(Va_{0.5}R^{2+}{}_{1.5}Ti)(Si_2Al_2)O_{10}(OH)_2$, where Va is vacancy in octahedral site and R^{2+} is Fe^{2+}, Mn or Mg. Thus, Ti is incorporated into biotite with the increase of vacancy in octahedral site. The complied data show a positive correlation between vacancy^{VI} and Ti content (Fig. 6). Biotite from the Caledonides contains a Ti-biotite component of up to ~20 mol%. Ti content of secondary biotite from the Sulu region is widely scattered and controlled by local bulk composition; i.e. biotite near rutile or ilmenite is high in Ti content. Eclogite-facies biotite in the Caledonides is richer in the Na-biotite component than nearly all the secondary biotite from the Sulu region (Fig. 6); the K content in biotite from the Caledonides ranges from 0.79 to 0.89 pfu, whereas that in secondary biotite from the Sulu region ranges from 0.83 to 0.99 pfu. Na-biotite content may increase with increasing pressure.

Discussion

As described above, biotite occurs in the Caledonian eclogite, whereas phengite commonly occurs in eclogites from the Dabie–Sulu region and other orogenic belts. Petrological data predicted that biotite and orthopyroxene would be stabilized in eclogite with Mg-rich picrite basalt composition. Garnet in the Bt- or Opx-bearing eclogites shows low Ca/Mg ratio, which is consistent with bulk compositional data. In order to confirm these petrological data, thermodynamic calculations were carried out on the stability of phengite, biotite and orthopyroxene. The aim of this calculation is not to obtain complete phase diagrams, but to obtain semi-quantitative results that show the relative relationship of the stability of these minerals, and, hence, several rough assumptions were employed. To deal with

the paragenesis of phengite and biotite in eclogite, we need at least an eight-component system: K_2O–Na_2O–CaO–FeO–MgO–Al_2O_3–SiO_2–H_2O, where Fe_2O_3 is ignored and TiO_2 is assumed to be contained only in rutile. To focus the discussion on K-mica, other hydrous phases such as amphibole and epidote as well as fluid, are ignored. Corundum and K-feldspar are rare in eclogitic rocks, and these phases are also ignored. In this proposed system, K_2O and H_2O are assumed to be present only in micas, ideally in the ratio 0.5 K_2O to H_2O and, hence, the system is transformed to a seven-component system $KH_2O_{1.5}$–Na_2O–CaO–FeO–MgO–Al_2O_3–SiO_2, which includes garnet, kyanite, phengite, biotite, quartz or coesite, omphacite, orthopyroxene and olivine (Ol). The assumed mineral formulae of these phases are shown in Table 4. Phengite is treated to have three end members: muscovite, celadonite and Fe-celadonite. Biotite is simplified to phlogopite-to-annite solid solution, although subordinate amounts of eastonite, Ti-biotite and Na-biotite components are contained in eclogite-facies biotite. For clinopyroxene, Ca-Tschermak, enstatite and Ca-eskolaite components would be important in high-T (>900 °C) conditions (Hermann 2002), but these components are ignored. Orthopyroxene is also simplified to enstatite-to-ferrosilite solid solution. The effects of all of these assumptions are uncertain, but these assumptions would not affect the relative relationship of the stability of phengite, biotite and orthopyroxene.

The thermodynamic dataset of Holland and Powell (1998) is used herein as it is the best available. However, this dataset quantitatively contradicts the observed petrography in some cases (e.g. Izadyar et al. 2000), and, hence, the calculated results should be semi-quantitative. The regular solution model is adopted to calculate activities of the phase components in garnet, biotite, orthopyroxene, clinopyroxene and olivine (Appendix), where excess interaction parameters mainly follow Holland and Powell (1998). The activity model for phengite is also from Holland and Powell (1998), and maintains the internal consistency of the thermodynamic dataset; i.e. enthalpy of celadonite in this dataset depends on this mixing model.

Garnet composition diagram

In the calculation, garnet is treated as always present in the system, and then petrogenetic grids are drawn on the garnet composition diagram (e.g. Hirajima et al. 1988); an almandine–grossular–pyrope triangle diagram. This diagram is a modified chemical potential diagram because the axes Fe/(Fe + Ca + Mg) and Ca/(Fe + Ca + Mg) are related to the chemical potential of almandine and grossular components in garnet, as described in Hirajima et al. (1988). Under constant P–T conditions, garnet associated with six phases has a fixed composition in the seven-component system, and, hence, an invariant point appears on the garnet composition diagram. Garnets associated with five and four phases have one and two degrees of freedom, respectively and, in these cases, either univariant curves or divariant fields appear on the diagram. Firstly, in order to clarify the geometry of the mineral parageneses on the garnet composition diagram, the divariant field in the above seven-component system is modified to a univariant curve in a Na_2O-free six-component system by treating omphacite as Na-free augite (Aug). The primary purpose of treating Na-free augite is not to simplify the calculations. It is necessary as a fundamental first step to clarify the geometry. Univariant curves and divariant fields in a Na_2O-bearing system are described later.

Under constant P–T conditions, a four-phase association + garnet has one degree of freedom in the six-component system, and creates a univariant curve in the garnet composition diagram. Quartz or coesite generally cannot coexist with olivine, and the association of QC + Ol should be unstable. We, therefore, have to consider Ol- or QC-free assemblages, and the following Ol- or QC-free invariant assemblages are obtained; [Ky, Ol], [Phn, Ol], [Bt, Ol], [QC, Ol], [Aug, Ol], [Opx, Ol], [Ky, QC], [Phn, QC], [Bt, QC], [Aug, QC] and [Opx, Qtz], where [α, β] represents an α- and β-free assemblage. Five univariant curves should radiate from each of the above 11 invariant points, but some of these curves coincide in the reduced component system (Table 5). For example, coexistence of three phases, Grt, Opx and Aug, has one degree of freedom in a four-component system: $CaSiO_3$–$FeSiO_3$–$MgSiO_3$–Al_2O_3. Therefore, in any univariant assemblages including Opx and Aug, garnet compositions are controlled by the existence of only Opx and Aug. Phases constraining the positions of univariant curves are listed in Table 5. To constrain the garnet compositions along each univariant curve, a set of several independent reactions was selected from reactions among end-member components (Table 6).

For example, for the univariant assemblage of Grt + Aug + Phn + Bt + Qtz (3) in Table 5 and Fig. 7, six independent compositional variables of X_{prp}, X_{grs}, X_{di}, X_{Mg}^{Phn}, y and X_{phl} exist, where X_i is the mole fraction of phase component i, X_{Mg}^{Phn} is $Mg/(Fe^{2+} + Mg)$ in phengite, and y is the mole fraction of the muscovite component. Then, five independent equations are selected from Table 6 as follows:

$$\text{Muscovite} + 2\text{Phlogopite} + 6\text{Quartz} = \text{Pyrope} + 3\text{Celadonite} \quad \text{(d)}$$

$$\text{Muscovite} + 6\text{Diopside} = \text{Pyrope} + 2\text{Grossular} + 3\text{Celadonite} \quad \text{(m)}$$

$$\text{FeMg}_{-1}(\text{Garnet}) = \text{FeMg}_{-1}(\text{Augite}) \quad \text{(q)}$$

$$\text{FeMg}_{-1}(\text{Garnet}) = \text{FeMg}_{-1}(\text{Phengite}) \quad \text{(r)}$$

$$\text{FeMg}_{-1}(\text{Garnet}) = \text{FeMg}_{-1}(\text{Biotite}). \quad \text{(s)}$$

Table 5 Invariant and univariant assemblages in the garnet composition diagrams. [α] α-absent assemblage. *Abbreviations* are listed in Table 4

Invariant	Univariant	Phases constraining Grt compositions
[Ky, Ol]	[Ky, Ol, Phn]	1: Opx + Aug
	[Ky, Ol, Bt]	1: Opx + Aug
	[Ky, Ol, Qtz/Coe]	1: Opx + Aug
	[Ky, Ol, Aug]	2: Bt + Qtz/Coe + Phn + Opx
	[Ky, Ol, Opx]	3: Bt + Qtz/Coe + Phn + Aug
[Phn, Ol]	[Phn, Ol, Ky]	1: Opx + Aug
	[Phn, Ol, Bt]	1: Opx + Aug
	[Phn, Ol, Qtz/Coe]	1: Opx + Aug
	[Phn, Ol, Aug]	4: Qtz/Coe + Ky + Opx
	[Phn, Ol, Opx]	5: Qtz/Coe + Ky + Aug
[Bt, Ol]	[Bt, Ol, Ky]	1: Opx + Aug
	[Bt, Ol, Phn]	1: Opx + Aug
	[Bt, Ol, Qtz/Coe]	1: Opx + Aug
	[Bt, Ol, Aug]	4: Qtz/Coe + Ky + Opx
	[Bt, Ol, Opx]	5: Qtz/Coe + Ky + Aug
[Qtz/Coe, Ol]	[Qtz/Coe, Ol, Ky]	1: Opx + Aug
	[Qtz/Coe, Ol, Phn]	1: Opx + Aug
	[Qtz/Coe, Ol, Bt]	1: Opx + Aug
	[Qtz/Coe, Ol, Aug]	6: Phn + Ky + Opx + Bt
	[Qtz/Coe, Ol, Opx]	7: Phn + Ky + Aug + Bt
[Aug, Ol]	[Aug, Ol, Ky]	2: Bt + Qtz/Coe + Phn + Opx
	[Aug, Ol, Phn]	4: Qtz/Coe + Ky + Opx
	[Aug, Ol, Bt]	4: Qtz/Coe + Ky + Opx
	[Aug, Ol, Qtz/Coe]	6: Phn + Ky + Opx + Bt
	[Aug, Ol, Opx]	8: Phn + Ky + Qtz/Coe + Bt
[Opx, Ol]	[Opx, Ol, Ky]	3: Bt + Qtz/Coe + Phn + Aug
	[Opx, Ol, Phn]	5: Qtz/Coe + Ky + Aug
	[Opx, Ol, Bt]	5: Qtz/Coe + Ky + Aug
	[Opx, Ol, Qtz/Coe]	7: Phn + Ky + Aug + Bt
	[Opx, Ol, Aug]	8: Phn + Ky + Qtz/Coe + Bt
[Ky, Qtz/Coe]	[Ky, Qtz/Coe, Phn]	1: Opx + Aug
	[Ky, Qtz/Coe, Bt]	1: Opx + Aug
	[Ky, Qtz/Coe, Ol]	1: Opx + Aug
	[Ky, Qtz/Coe, Aug]	9: Ol + Bt + Phn + Opx
	[Ky, Qtz/Coe, Opx]	10: Ol + Bt + Phn + Aug
[Phn, Qtz/Coe]	[Phn, Qtz/Coe, Ky]	1: Opx + Aug
	[Phn, Qtz/Coe, Bt]	1: Opx + Aug
	[Phn, Qtz/Coe, Ol]	1: Opx + Aug
	[Phn, Qtz/Coe, Aug]	11: Ol + Ky + Opx
	[Phn, Qtz/Coe, Opx]	12: Ol + Ky + Aug
[Bt, Qtz/Coe]	[Bt, Qtz/Coe, Ky]	1: Opx + Aug
	[Bt, Qtz/Coe, Phn]	1: Opx + Aug
	[Bt, Qtz/Coe, Ol]	1: Opx + Aug
	[Bt, Qtz/Coe, Aug]	11: Ol + Ky + Opx
	[Bt, Qtz/Coe, Opx]	12: Ol + Ky + Aug
[Aug, Qtz/Coe]	[Aug, Qtz/Coe, Ky]	9: Ol + Bt + Phn + Opx
	[Aug, Qtz/Coe, Phn]	11: Ol + Ky + Opx
	[Aug, Qtz/Coe, Bt]	11: Ol + Ky + Opx
	[Aug, Qtz/Coe, Ol]	6: Phn + Ky + Opx + Bt
	[Aug, Qtz/Coe, Opx]	13: Ol + Bt + Phn + Ky
[Opx, Qtz/Coe]	[Opx, Qtz/Coe, Ky]	10: Ol + Bt + Phn + Aug
	[Opx, Qtz/Coe, Phn]	12: Ol + Ky + Aug
	[Opx, Qtz/Coe, Bt]	12: Ol + Ky + Aug
	[Opx, Qtz/Coe, Ol]	7: Phn + Ky + Aug + Bt
	[Opx, Qtz/Coe, Aug]	13: Ol + Bt + Phn + Ky

For each independent endmember reaction, a thermodynamic equilibrium equation is written; e.g. Eq. (d) $\mu_{muscovite} + 2\ \mu_{phlogopite} + 6\ \mu_{quartz} = \mu_{pyrope} + 3\ \mu_{celadonite}$, where μ_i is the chemical potential of phase component i. Thus, five equations and six variables are present in this case. Therefore, by solving the thermodynamic equations for the above five reactions simultaneously, a relation of $f(X_{prp}, X_{grs}) = 0$ is obtained, and a univariant curve can be drawn on the garnet composition diagram. Then, to determine the stable side for each phase, the free energy of a phase is slightly reduced, and then the stability field of that phase should expand. For all of the univariant assemblages (Table 5), similar calculations were carried out and all univariant curves drawn on the garnet composition diagram. The phase diagram is finally constructed by applying Schreinemaker's rules.

An almandine–grossular–pyrope diagram (Fig. 7) illustrates mineral parageneses at 700 °C, 2.5 GPa.

Table 6 Reactions among endmember components of the phases in Table 4 to constrain mineral compositions. Na_2O is contained only in omphacite in this model system, and Na-bearing phase component is only jadeite. Therefore, Na-bearing end-member reaction does not exist

$KH_2O_{1.5}$–CaO–MgO–Al_2O_3–SiO_2system
(a) Phlogopite + 3 Quartz = Celadonite + Enstatite
(b) 2 Pyrope + 2 Quartz = 3 Enstatite + 2 Kyanite
(c) 3 Phlogopite + 2 Kyanite + 7 Quartz = 2 Pyrope + 3 Celadonite
(d) Muscovite + 2 Phlogopite + 6 Quartz = Pyrope + 3 Celadonite
(e) Muscovite + 2 Enstatite = Pyrope + Celadonite
(f) 3 Celadonite + 4 Kyanite = Pyrope + 3 Muscovite + 4 Quartz
(g) Phlogopite + 2 Kyanite + Quartz = Pyrope + Muscovite
(h) 2 Phlogopite + 2 Kyanite + 4 Quartz = 2 Muscovite + 3 Enstatite
(i) Muscovite + 3 Enstatite = Pyrope + Phlogopite + 3 Quartz
(j) 3 Celadonite + 4 Phlogopite + 12 Kyanite = 5 Pyrope + 7 Muscovite
(k) 3 Forsterite + Muscovite = Pyrope + Phlogopite
(l) 2 Forsterite + 2 Kyanite + Enstatite = 2 Pyrope
(m) 3 Muscovite + 6 Diopside = Pyrope + 2 Grossular + 3 Celadonite
(n) Grossular + Pyrope + 2 Quartz = 3 Diopside + 2 Kyanite
(o) Grossular + 3 Enstatite = Pyrope + 3 Diopside
(p) 3 Diopside + 6 Forsterite + 6 Kyanite = 5 Pyrope + Grossular
Fe–Mg exchange reactions
(q) $FeMg_{-1}$ (Garnet) = $FeMg_{-1}$ (Omphacite)
(r) $FeMg_{-1}$ (Garnet) = $FeMg_{-1}$ (Phengite)
(s) $FeMg_{-1}$ (Garnet) = $FeMg_{-1}$ (Biotite)
(t) $FeMg_{-1}$ (Garnet) = $FeMg_{-1}$ (Orthopyroxene)
(u) $FeMg_{-1}$(Garnet) = $FeMg_{-1}$ (Olivine)

None of the univariant assemblages that include olivine appear on the garnet composition diagram. Biotite + quartz is stable in the grossular-poor field: i.e. vertically striped field in Fig. 7. Orthopyroxene is also stable in grossular-poor field bounded by univariant curve (1), as predicted by Banno (1965). When Na_2O is incorporated into augite, the system becomes a seven-component system. Invariant points, ia, ib and ic (Fig. 7), in the six-component system change to univariant curves in the seven-component system. The univariant curves in the Na_2O-bearing seven-component system correspond to univariant curves (2), (4) and (6) in Fig. 7 because Na_2O is assumed to be absent from all phases except omphacite in the present model. For example, for the univariant assemblage Grt + Omp + Opx + Phn + Bt + Qtz in the seven-component system, excluding omphacite, six independent compositional variables, X_{prp}, X_{grs}, X_{en}, X_{Mg}^{Phn}, y and X_{phl}, exist. Then, five independent equations are selected from Table 6 as follows:

$$\text{Phlogopite} + 3\text{Quartz} = \text{Celadonite} + \text{Enstatite} \quad \text{(a)}$$

$$\text{Muscovite} + 2\text{Enstatite} = \text{Pyrope} + \text{Celadonite} \quad \text{(e)}$$

Eqs. (r), (s) and

$$FeMg_{-1}(\text{Garnet}) = FeMg_{-1}(\text{Orthopyroxene}). \quad \text{(t)}$$

Thus, excluding omphacite, five equations and six variables are present. Therefore, by solving the five equations simultaneously, an equation of $f(X_{prp}, X_{grs}) = 0$ is obtained. Thus, garnet compositions are controlled only by the Opx + Phn + Bt + Qtz assemblage, which corresponds to univariant curve (2) in Fig. 7. The presence of omphacite does not affect the position of univariant curves (2), (4) and (6). Adding the independent variables X_{di} and X_{jd} for omphacite, two independent equations, Eqs. (m) and (q) are selected to determine the composition of omphacite along univariant curve (2).

The activity of the diopside component (a_{di}) is expressed as $a_{di} = X_{di}\ \exp[300(1-X_{di}-X_{jd})(1-X_{di})/T]$, and that of the hedenbergite component (a_{hd}) is expressed as $a_{hd} = (1-X_{jd}-X_{di})\ \exp[300X_{di}\ (X_{di}+X_{jd})/T]$ (Appendix). Thus, the two variables X_{di} and X_{jd} and the two related equations are given, and, hence, the values of X_{di} and X_{jd} can be determined by solving the above two equations simultaneously. Along univariant curves (2), (4) and (6), the jadeite content of clinopyroxene gradually increases from invariant point ia, ib and ic, respectively (Fig. 7); however, the positions of these univariant curves do not shift.

Univariant curves in the six-component system that include augite become divariant fields in the Na-bearing seven-component system. Univariant curves (1), (3), (5) and (7) in the Na-free system convert to clinopyroxene-stable fields that expand with increasing jadeite content. The iso-X_{jd} curves for $X_{jd} = 0.40$ in the divariant assemblages are shown on the garnet composition diagram in Fig. 7. Thus, the stability fields of Phn + Aug and Aug, which are bounded by univariant curves (3) and (1), respectively, expand with increasing jadeite content, and, hence, the stability fields of Bt + Qtz and Opx shrink in a Na-bearing system. Thus, biotite + quartz occurs with Ca-poor garnet, and the stability field of orthopyroxene is also limited to the Ca-poor side on the garnet composition diagram (Fig. 7). These are consistent with observational data on natural eclogite: most data for garnet in Bt- or Opx-bearing eclogites from the Caledonides are poor in Ca (Fig. 4). Furthermore, the Bt- or Opx-bearing eclogites do not contain kyanite (Table 2). The calculated phase relation shows

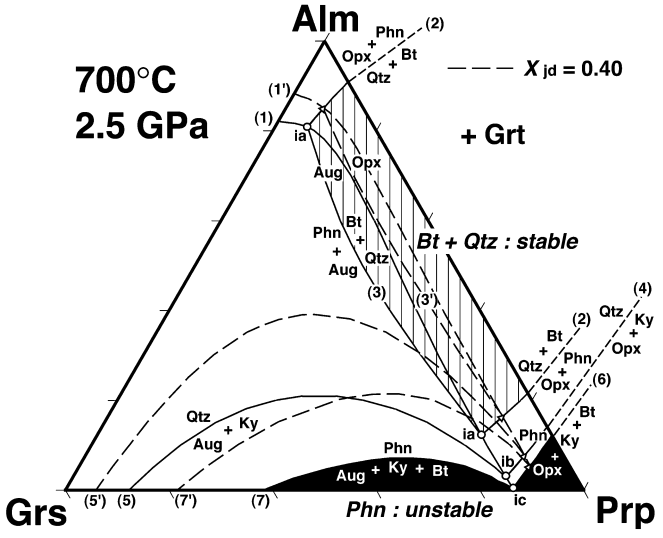

Fig. 7 Garnet composition diagram showing the calculated mineral parageneses at 700 °C, 2.5 GPa. This diagram was mainly constructed in the $KH_2O_{1.5}$–CaO–FeO–MgO–Al_2O_3–SiO_2 system. Label number of univariant curves is the same as that in Table 5. The association of biotite + quartz is stable, when the composition of the coexisting garnet is in the vertically-striped field, where grossular content is low. This field is bounded by univariant curves (2) and (3). Stability field of orthopyroxene is also restricted to grossular-poor compositions, which is bounded by univariant curve (1). Invariant points *ia*, *ib* and *ic* change to univariant curves in Na_2O-bearing system, which correspond univariant curves (2), (4) and (6), respectively. Positions of these curves are not different from Na_2O-free system because phases except for clinopyroxene are not assumed to contain Na_2O in this model. Along univariant curves (2), (4) and (6) from invariant points *ia*, *ib* and *ic*, jadeite content of coexisting clinopyroxene gradually increases. Univariant curves (1), (3), (5) and (7) change to divariant fields in Na_2O-bearing system. With increasing jadeite content in clinopyroxene [X_{jd}: Na/(Ca + Na)], augite-stable side on univariant curves (1), (3), (5) and (7) gradually expand. Iso-X_{jd} (= 0.40) curves (1′), (3′), (5′) and (7′) are drawn for divariant assemblages (1), (3), (5) and (7) in Na_2O-bearing system, respectively. *Alm* Almandine; *Grs* grossular; *Prp* pyrope. The other *abbreviations* are the same as in Table 4

that stability field of Omp + Ky + Bt is restricted to the Fe-poor part [roughly bounded by iso-X_{jd} curve (7') in Fig. 7], and hence kyanite rarely occurs in Bt-bearing eclogitic rocks. The association of Ky + Opx is only stable with pyrope-rich (> 85%) garnet (Fig. 7), and this is an unrealistic assemblage in usual eclogitic rocks. However, the association of Ky + Opx is actually present within pyrope-rich garnet ($X_{prp} = 0.86$–0.94; $X_{alm} = 0.11 = 0.05$; $X_{grs} = 0.01$–0.03) from the UHP unit of Dora Maira massif, the western Alps (Simon and Chopin 2001), which is consistent with the calculated result.

Figure 8 shows the stability relationships among these phases from 700 to 900 °C, and from 2.5 to 3.5 GPa. The stability field of Bt + QC expands with increasing temperature and decreasing pressure. Under low-T and high-P conditions, the stability field of Bt + QC is absent, as shown in the diagram at 700 °C, 3.5 GPa (Fig. 8). In contrast, the Opx-stable field is mostly independent of the variation in P–T conditions. This is also consistent with observations of Caledonian eclogites that biotite occurs in eclogites mainly from the higher-grade part of the Caledonides, whereas Opx-bearing eclogites occur both in the lower- and higher-grade parts of the WGR.

Pseudosection

Changes in the mineral assemblage and the modes of the constituents were calculated using bulk compositions in the $KH_2O_{1.5}$–Na_2O–CaO–FeO–MgO–Al_2O_3–TiO_2–SiO_2 system, including Grt, Ky, Phn, Bt, QC, Omp, Opx, Ol and Rt. The thermodynamic dataset used was also of Holland and Powell (1998). In this calculation, not only the variability in mineral compositions, but also that in the modal per cents, should be constrained. In addition to the thermodynamic equilibrium equations for the reactions in Table 6, seven additional equations were prepared for the mass balance of constituents in the system. For example, the mole quantity of K should be equal to that of Phn + Bt in a given bulk composition, as defined by the equation:

$$N(\mathrm{K}) = N(\mathrm{Phn}) + N(\mathrm{Bt}) \quad \text{(I)}$$

where $N(\alpha)$ is the mole quantity of α in the system. The other mass-balance equations can be written as follows:

$$N(\mathrm{Na}) = N(\mathrm{Omp})X_{jd} \quad \text{(II)}$$

$$N(\mathrm{Ca}) = 3N(\mathrm{Grt})X_{\mathrm{grs}} + N(\mathrm{Omp})(1 - X_{\mathrm{jd}}) \quad \text{(III)}$$

$$\begin{aligned} N(\mathrm{Fe} + \mathrm{Mg}) = {} & 3N(\mathrm{Grt})(1 - X_{\mathrm{grs}}) + N(\mathrm{Omp})(1 - X_{\mathrm{jd}}) \\ & + 2N(\mathrm{Opx}) + 2N(\mathrm{Ol}) + N(\mathrm{Phn})(1 - y) \\ & + 3N(\mathrm{Bt}) \end{aligned} \quad \text{(IV)}$$

$$\begin{aligned} N(\mathrm{Mg}) = {} & 3\mathrm{N}(\mathrm{Grt})X_{\mathrm{prp}} + N(\mathrm{Omp})\,X_{\mathrm{di}} + 2N(\mathrm{Opx})X_{\mathrm{en}} \\ & + 2N(\mathrm{Ol})X_{\mathrm{fo}} + N(\mathrm{Phn})(1 - y)X_{\mathrm{Mg}}^{\mathrm{Phn}} \\ & + 3N(\mathrm{Bt})X_{\mathrm{phl}} \end{aligned} \quad \text{(V)}$$

$$\begin{aligned} N(\mathrm{Al}) = {} & 2N(\mathrm{Grt}) + N(\mathrm{Omp})X_{\mathrm{jd}} + N(\mathrm{Phn})(2y + 1) \\ & + N(\mathrm{Bt}) + 2N(\mathrm{Ky}) \end{aligned} \quad \text{(VI)}$$

$$\begin{aligned} N(\mathrm{Si}) = {} & 3N(\mathrm{Grt}) + 2N(\mathrm{Omp}) + 2N(\mathrm{Opx}) + N(\mathrm{Ol}) \\ & + N(\mathrm{Phn})(4 - y) + 3N(\mathrm{Bt}) + N(\mathrm{Ky}) + N(\mathrm{Qtz}) \end{aligned} \quad \text{(VII)}$$

TiO_2 is assumed to be contained only in rutile.

Using the above mass-balance equations and the equations in Table 6, the variabilities of composition and mode were determined for all mineral assemblages. For example, in the case of the assemblage Grt + Omp + Phn + Qtz, there are ten independent variables: X_{prp}, X_{grs}, X_{jd}, X_{di}, X_{Mg}^{Phn}, y, N(Grt), N(Omp), N(Phn) and

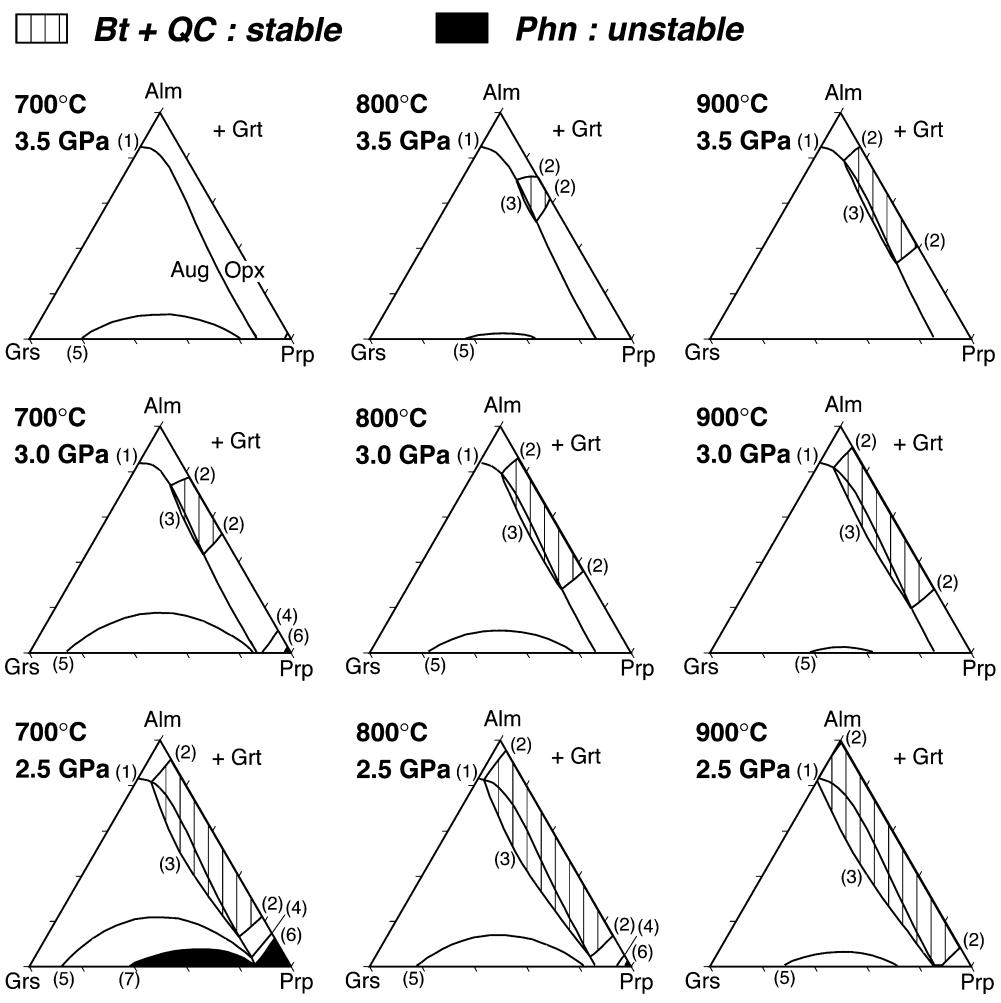

Fig. 8 Calculated garnet composition diagrams at 700–900 °C, 2.5–3.5 GPa in the $KH_2O_{1.5}$–CaO–FeO–MgO–Al_2O_3–SiO_2 system. *Label number of univariant curves* in this figure is the same as those shown in Fig. 7. The *vertically striped field* shows the biotite (Bt) + quartz or coesite (QC) stable composition of garnet. The Bt + QC stable field expands with increasing temperature and decreasing pressure. However, orthopyroxene-stable field bounded by univariant curve (1) is mostly independent of P–T conditions. *Abbreviations* are the same as in Fig. 7

N(Qtz), at any given P–T conditions. Then, ten independent thermodynamic and mass-balance equations can be written as follows:

$$3\mu_{\text{muscovite}} + 6\mu_{\text{diopside}} = \mu_{\text{pyrope}} + 2\mu_{\text{grossular}} + 3\mu_{\text{celadonite}} \quad (\text{m}')$$

$$\mu_{\text{almandine}} + 3\mu_{\text{diopside}} = \mu_{\text{pyrope}} + 3\mu_{\text{hedenbergite}} \quad (\text{q}')$$

$$\mu_{\text{almandine}} + 3\mu_{\text{celadonite}} = \mu_{\text{pyrope}} + 3\mu_{\text{Fe-celadonite}} \quad (\text{r}')$$

$$N(\text{K}) = N(\text{Phn}) \quad (\text{I}')$$

$$N(\text{Na}) = N(\text{Omp})\, X_{\text{jd}} \quad (\text{II}')$$

$$N(\text{Ca}) = 3N(\text{Grt})\, X_{\text{grs}} + N(\text{Omp})(1 - X_{\text{jd}}) \quad (\text{III}')$$

$$N(\text{Fe} + \text{Mg}) = 3N(\text{Grt})(1 - X_{\text{grs}}) + N(\text{Omp})(1 - X_{\text{jd}}) + N(\text{Phn})(1 - y) \quad (\text{IV}')$$

$$N(\text{Mg}) = 3N(\text{Grt})\, X_{\text{prp}} + N(\text{Omp})\, X_{\text{di}} + N(\text{Phn})(1 - y)\, X_{\text{Mg}}^{\text{Phn}} \quad (\text{V}')$$

$$N(\text{Al}) = 2N(\text{Grt}) + N(\text{Omp})\, X_{\text{jd}} + N(\text{Phn})(2y + 1) \quad (\text{VI}')$$

$$N(\text{Si}) = 3N(\text{Grt}) + 2N(\text{Omp}) + N(\text{Phn})\,(4 - y) + N(\text{Qtz}) \quad (\text{VII}')$$

By solving the above ten independent equations simultaneously, the magnitudes of all of the above ten variables, compositions and mole quantities of the coexisting phases, are determined for any bulk composition. Total Gibbs free energy of the system can, therefore, be obtained. This type of calculation was carried out for all of the possible mineral assemblages at a given bulk composition. Then, the stable mineral assemblage was determined in the following order: (1) assemblages yielding negative values for variables are excluded from the calculation of Gibbs free energy; and (2) a search is carried out for the mineral assemblage giving the minimum Gibbs free energy. This is taken as the stable assemblage under each set of conditions. For any given bulk composi-

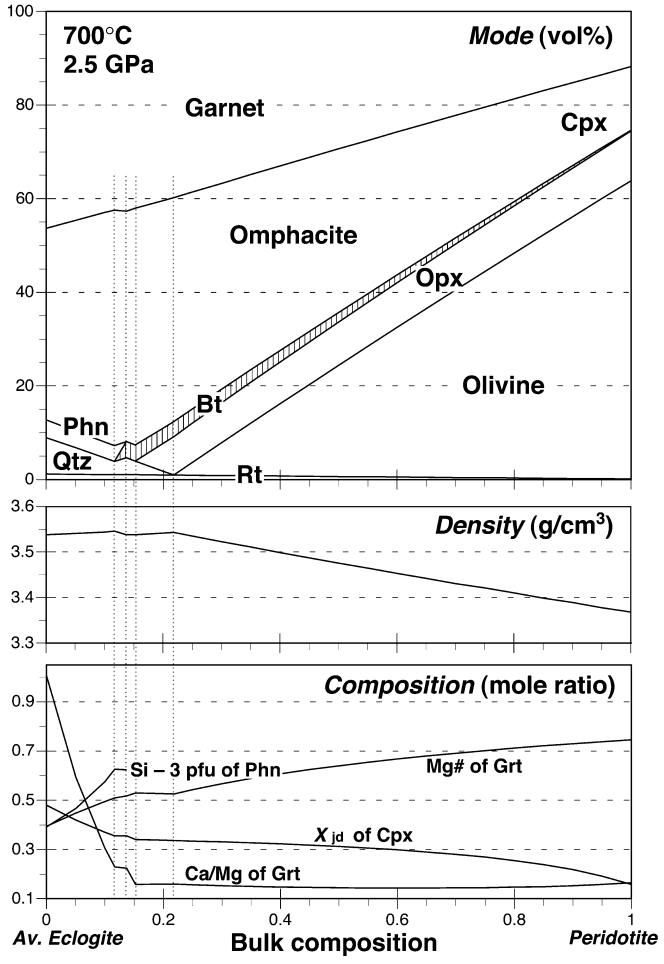

Fig. 9 Variation of modes of the constituent minerals (vol%), density, and mineral compositions related to bulk compositions ranging from the Av. eclogite to the peridotite (KLB-1; Table 3), which were calculated in the $KH_2O_{1.5}$–Na_2O–CaO–FeO–MgO–Al_2O_3–TiO_2–SiO_2 system. TiO_2 was assumed to be contained only in rutile (*Rt*). The Av. eclogite is the average bulk composition of the Dabie–Sulu eclogites (Fig. 3). The calculated P–T conditions are 700 °C, 2.5 GPa. Under bulk compositions of 0–12% peridotite + 100–88% Av. eclogite by weight, phengite is a stable hydrous K phase, whereas under bulk compositions of 12–100% peridotite + 88–0% Av. eclogite by weight, biotite is stable. As the peridotite component was incorporated into the Av. eclogite, orthopyroxene and olivine were stabilized when the peridotite component reached 15.5 and 21.8 wt%, respectively. In the biotite-stable bulk compositions, the Ca/Mg mole ratio of garnet is ≤ 0.23. Mg#: Mg/(Fe + Mg) mole ratio of garnet. X_{jd}: Na/(Na + Ca) mole ratio of clinopyroxene (*Cpx*). The other abbreviations are the same as in Table 4

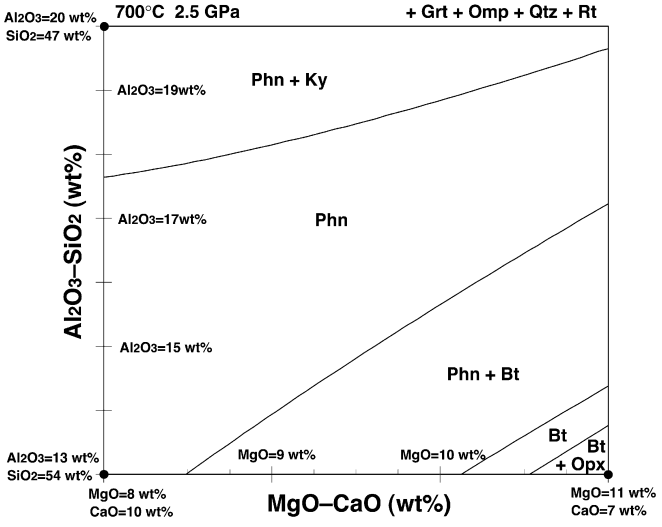

Fig. 10 Calculated variation of mineral assemblage in MgO–CaO versus Al_2O_3–SiO_2 (wt%) bulk compositional space at 700 °C, 2.5 GPa, where TiO_2, FeO, Na_2O and K_2O contents were fixed to be 1.00, 11.00, 2.00 and 1.00 wt%, respectively. The calculation method is the same as in Fig. 9. The MgO and CaO contents were changed from 8.00 and 10.00 to 11.00 and 7.00 wt%, respectively, and the Al_2O_3 and SiO_2 contents were also changed from 13.00 and 54.00 to 20.00 and 47.00 wt%, respectively. In this compositional space, garnet, omphacite, quartz and rutile are commonly present. Biotite and orthopyroxene were stabilized in MgO-rich and CaO- and Al_2O_3-poor bulk compositions. The *abbreviations* are the same as in Table 4

tion and P–T conditions, this procedure gives the stable mineral assemblages, their amounts and mineral compositions.

Firstly, calculations were performed for bulk compositions ranging from the Av. eclogite to the peridotite composition (KLB-1; Table 3). Figure 9 shows the result of these calculations at 700 °C and 2.5 GPa. At compositions approximating to the Av. eclogite, phengite is the stable K phase. The bulk composition is then changed by adding peridotite component. Biotite appears at compositions having the peridotite component of 12 wt%, and orthopyroxene appears when the peridotite component reaches 15.5 wt% (Fig. 9). The modal percentage of quartz decreases as the peridotite component increases. Olivine appears at compositions having ≥ 22% peridotite component by weight. The occurrence of biotite and orthopyroxene in eclogites from the WGR is consistent with the result of this calculation: the bulk compositions of these rocks are close to compositions with the peridotite component of ≈20 wt% (Fig. 3).

The density of eclogite-to-peridotite, and the Ca/Mg and Mg/(Fe + Mg) (Mg#) mole ratio of garnet, the Na/(Ca + Na) ratio of omphacite (X_{jd}) and Si content of phengite (Si–3 pfu) were also calculated and shown in Fig. 9. The density does not significantly change with the variation in bulk composition for quartz-bearing assemblages (3.542 ± 0.004 g/cm^3; Fig. 9). However, for the quartz-free assemblage, with a decrease in the modal percentage of garnet, the density significantly decreases and reaches 3.37 g/cm^3 at the peridotite composition (Fig. 9). The Si content of phengite increases from 3.39 to 3.62 pfu with increasing the peridotite component. Although the Si content of phengite generally increases with increasing pressure and decreasing temperature, as experimentally shown by Schmidt and Poli (1998), variations in bulk composition also significantly affect the Si content of phengite. The Ca/Mg mole ratio of

garnet decreases from 1.01 to 0.16 as the peridotite component increases from 0 to 20 wt%, and the Ca/Mg mole ratio of garnet is ≤ 0.23 in the biotite-stable bulk compositions (Fig. 9). The compiled Ca/Mg mole ratios of garnet from the WGR range from 0.17 to 0.34, which is close to the value calculated for the biotite-stable range.

The above calculations showed that biotite and orthopyroxene should be stable in eclogite with picrite basaltic compositions, but it is not clear which chemical components are related to the stabilization of biotite and orthopyroxene in eclogite. As summarized in the previous section (Table 2), biotite and orthopyroxene are stable even in quartz-saturated eclogites, indicating that decrease of SiO_2 content is irrelevant to the stabilization of biotite and orthopyroxene in eclogites. The compilation of bulk compositional data suggested that low CaO/MgO ratio in bulk composition should be an important factor for stabilizing of biotite and orthopyroxene in eclogites. Bt-bearing eclogite from NEGEP is extremely poor in Al_2O_3 (Fig. 3), and hence such Al-poor environments also stabilize biotite in eclogite. To clarify these observational data, calculations were done for MgO–CaO versus Al_2O_3–SiO_2 (wt%) bulk compositional space at 700 °C, 2.5 GPa (Fig. 10), where TiO_2, FeO, Na_2O and K_2O contents were fixed to be 1.00, 11.00, 2.00 and 1.00 wt%, respectively. The MgO and CaO contents were changed from 8.00 and 10.00 to 11.00 and 7.00 wt%, respectively, which corresponds to horizontal vector in Fig. 10. The Al_2O_3 and SiO_2 contents were also changed from 13.00 and 54.00 to 20.00 and 47.00 wt%, respectively, which is vertical vector in Fig. 10. As a result of the calculations, biotite and orthopyroxene were stabilized in MgO-rich and CaO- and Al_2O_3-poor bulk compositions. When Al_2O_3 content is high (e.g. >17 wt%), biotite and orthopyroxene are unstable even in MgO-rich and CaO-poor environments (Fig. 10). On the other hand, biotite and orthopyroxene do not occur even in Al_2O_3-poor environments, when CaO/MgO ratio is relatively high (e.g. MgO $\approx$8 wt%, CaO $\approx$10 wt%). Thus, all of the MgO, CaO and Al_2O_3 contents are related to the stabilization of biotite and orthopyroxene. Bulk compositions should be low both in Al_2O_3 content and CaO/MgO ratio to stabilize biotite and orthopyroxene in eclogites. Kyanite was stabilized in Al_2O_3-rich bulk compositions (>18 wt%), and, hence, kyanite should not be accompanied by biotite and orthopyroxene in usual eclogitic rocks, except for extremely Mg-rich environments (Simon and Chopin 2001).

Conclusions

Phengite is a stable hydrous phase in many eclogites from representative orogenic belts, but biotite occurs in eclogites from several localities of the Caledonides. Occurrence of Opx-bearing eclogites is another feature of the Caledonides. These Bt- or Opx-bearing eclogites are similar to picrite basalts in bulk composition, suggesting that biotite and orthopyroxene should be stable in eclogite with picrite basaltic compositions. Bt- or Opx-bearing eclogites from the WGR are rich in MgO (10–15 wt%) and relatively poor in CaO and Al_2O_3. Bt-bearing eclogite from the NEGEP is also rich in MgO and extremely poor in Al_2O_3, but CaO content is rather high. Garnet in the Bt- or Opx-bearing eclogites is poor in the grossular component. Thermodynamic calculations for the multi-component system indicated that garnet compositions stable with Bt + Qtz and Opx are restricted to low-Ca field. Furthermore, thermodynamic calculations with mass-balance calculations confirmed that phengite should be stable in the 'ordinary' basaltic system whereas biotite and orthopyroxene should be stable in the picrite basaltic compositions; biotite and orthopyroxene were stabilized in eclogites with MgO-rich and CaO- and Al_2O_3-poor bulk compositions. Thus, the observational data are well consistent with the calculated results, although the calculations were performed with several rough assumptions. In picrite basaltic compositions, the mineral assemblage of eclogite should be completely different from that in 'ordinary' basaltic compositions. Depending on bulk composition, biotite may be stabilized instead of phengite even in rocks of basaltic compositions.

Acknowledgements I deeply thank E. Takahashi for his advice and encouragement at the Tokyo Institute of Technology, and I also thank T. Hirajima, S. Banno and S.R. Wallis for useful comments and for reviewing the manuscript. Thanks are also due to P.J. O'Brien for his useful advice. Critical comments from J. Hermann and an anonymous reviewer and editorial work by V. Trommsdorff are gratefully acknowledged. I would also thank T. Shinozaki for supporting the XRF analysis at the Tokyo Institute of Technology. Samples of the Dabie–Sulu region were collected as part of a project of Kyoto University supported by JSPS. A JSPS Research Fellowship for Young Scientists supported this study.

Appendix

Activity models for the model calculations

Garnet:

$$RT\ln a_{\mathrm{alm}} = RT\ln\,(X_{\mathrm{alm}})^3 + W_{\mathrm{alm-prp}}X_{\mathrm{prp}}(X_{\mathrm{prp}} + X_{\mathrm{grs}}) - W_{\mathrm{prp-grs}}\,X_{\mathrm{prp}}\,X_{\mathrm{grs}}$$

$$RT\ln a_{\mathrm{prp}} = RT\ln(X_{\mathrm{prp}})^3 + W_{\mathrm{alm-prp}}X_{\mathrm{alm}}(X_{\mathrm{alm}} + X_{\mathrm{grs}}) + W_{\mathrm{prp-grs}}X_{\mathrm{grs}}(X_{\mathrm{alm}} + X_{\mathrm{grs}})$$

$$RT\ln a_{\mathrm{grs}} = RT\ln(X_{\mathrm{grs}})^3 - W_{\mathrm{alm-prp}}X_{\mathrm{alm}}X_{\mathrm{prp}} + W_{\mathrm{prp-grs}}X_{\mathrm{prp}}(X_{\mathrm{alm}} + X_{\mathrm{prp}})$$

$$(W_{\mathrm{alm-prp}} = 2.4\mathrm{kJ};\ W_{\mathrm{prp-grs}} = 33\ \mathrm{kJ})$$

Phengite:

$$RT \ln a_{\mathrm{ms}} = RT \ln y^2(2-y)$$

$$RT \ln a_{\mathrm{cel}} = RT \ln\{0.25(1-y)(2-y)^2 \times [\mathrm{Mg}/(\mathrm{Fe}^{2+}+\mathrm{Mg})]\}$$

$$RT \ln a_{\mathrm{fcel}} = RT \ln\{0.25(1-y)(2-y)^2 \times [\mathrm{Fe}^{2+}/(\mathrm{Fe}^{2+}+\mathrm{Mg})]\}$$

($y = X_{\mathrm{Al}}^{\mathrm{M2A}}$: mole fraction of ms component)

Biotite:

$$RT \ln a_{\mathrm{phl}} = RT \ln(X_{\mathrm{phl}})^3 + W_{\mathrm{ann-phl}}(1-X_{\mathrm{phl}})^2$$

$$RT \ln a_{\mathrm{ann}} = RT \ln(1-X_{\mathrm{phl}})^3 + W_{\mathrm{ann-phl}}(X_{\mathrm{phl}})^2$$

($W_{\mathrm{ann-phl}} = 9$ kJ)

Orthopyroxene:

$$RT \ln a_{\mathrm{en}} = RT \ln(X_{\mathrm{en}}) + W_{\mathrm{en-fs}}(1-X_{\mathrm{en}})^2$$

$$RT \ln a_{\mathrm{fs}} = RT \ln(1-X_{\mathrm{en}}) + W_{\mathrm{en-fs}}(X_{\mathrm{en}})^2$$

($W_{\mathrm{en-fs}} = 0.5$ kJ)

Clinopyroxene:

$$RT \ln a_{\mathrm{di}} = RT \ln(X_{\mathrm{di}}) + W_{\mathrm{di-hd}} X_{\mathrm{hd}}(X_{\mathrm{hd}} + X_{\mathrm{jd}})$$

$$RT \ln a_{\mathrm{hd}} = RT \ln(X_{\mathrm{hd}}) + W_{\mathrm{di-hd}} X_{\mathrm{di}}(X_{\mathrm{di}} + X_{\mathrm{jd}})$$

($W_{\mathrm{di-hd}} = 2.5$ kJ)

Olivine:

$$RT \ln a_{\mathrm{fo}} = RT \ln(X_{\mathrm{fo}})^2 + W_{\mathrm{fo-fa}}(1-X_{\mathrm{fo}})^2$$

$$RT \ln a_{\mathrm{fa}} = RT \ln(1-X_{\mathrm{fo}})^2 + W_{\mathrm{fo-fa}}(X_{\mathrm{fo}})^2$$

($W_{\mathrm{fo-fa}} = 8.4$ kJ),

where R is the gas constant, T is temperature. a_{i} is the activity of the phase component i, and W_{i-j} is an excess interaction parameter between phase components i and j. X_{i} is the mole fraction of the phase component i. For garnet, symmetrical excess interaction energies between Fe and Mg and between Ca and Mg are included. Phengite is treated as a hypothetical Mg–Al fully ordered mica, and mixing of tetrahedral Al and Si is restricted to two of the four tetrahedral sites to maintain Al-avoidance. Excess interaction energy between muscovite and celadonite is close to zero within error (Holland and Powell 1998). For the other phases, only Fe–Mg excess interaction is introduced, and single-site mixing model is adopted for pyroxenes. Abbreviations are as follows: *alm* almandine; *prp* pyrope; *grs* grossular; *ms* muscovite; *cel* celadonite; *fcel* Fe-celadonite; *phl* phlogopite; *ann* annite; *en* enstatite; *fs* ferrosilite; *di* diopside; *hd* hedenbergite; *jd* jadeite; *fo* forsterite; *fa* fayarite.

References

Alt JC, Honnorez J, Laverne C, Emmermann R (1986) Hydrothermal alteration of a 1 km section through the upper oceanic crust, deep sea drilling project hole 504B; mineralogy, chemistry, and seawater-basalt interactions. J Geophys Res 91:10309–10335

Banno S (1965) Garnet–pyroxene equilibrium in granulite facies rocks and inclusions in kimberlite and alkali basalt. Jpn J Geol Geogr 36:23–36

Brothers RN, Yokoyama K (1982) Comparison of the high-pressure schist belts of New Caledonia and Sanbagawa, Japan. Contrib Mineral Petrol 79:219–229

Brueckner HK, Gilotti JA, Nutman AP (1998) Caledonian eclogite-facies metamorphism of early Proterozoic protoliths from the North-East Greenland eclogite province. Contrib Mineral Petrol 130:103–120

Carswell DA, O'Brien PJ, Wilson RN, Zhai M (1997) Thermobarometry of phengite-bearing eclogites in the Dabie Mountains of central China. J Metamorph Geol 15:239–252

Carswell DA, Wilson RN, Zhai M (2000) Metamorphic evolution, mineral chemistry and thermobarometry of schists and orthogneisses hosting ultra-high pressure eclogites in the Dabieshan of central China. Lithos 52:121–155

Chavagnac V, Jahn B (1996) Coesite-bearing eclogites from the Bixiling Complex, Dabie Mountains, China: Sm–Nd ages, geochemical characteristics and tectonic implications. Chem Geol 133:29–51

Chopin C, Henry C, Michard A (1991) Geology and petrology of the coesite-bearing terrain, Dora Maira massif, Western Alps. Eur J Mineral 3:263–291

Clarke GL, Aitchison JC, Cluzel D (1997) Eclogites and blueschists of the Pam Peninsula, NE New Caledonia: a reappraisal. J Petrol 38:843–876

Compagnoni R, Hirajima T, Chopin C (1995) Ultra-high-pressure metamorphic rocks in the western Alps. In: Coleman RG, Wang X (eds) Ultrahigh-pressure metamorphism. Cambridge University Press, Cambridge, pp 206–243

Cuthbert SJ, Carswell DA, Krogh-Ravna EJ, Wain A (2000) Eclogites and eclogites in the Western Gneiss Region, Norwegian Caledonides. Lithos 52:165–195

Domanik KJ, Holloway JR (1996) The stability and composition of phengitic muscovite and associated phases from 5.5 to 11 GPa: implications for deeply subducted sediments. Geochim Cosmochim Acta 60:4133–4150

Domanik KJ, Holloway JR (2000) Experimental synthesis and phase relations of phengitic muscovite from 6.5 to 11 GPa in a calcareous metapelite from the Dabie Mountains, China. Lithos 52:51–77

Droop GTR, Lombardo B, Pognante U (1990) Formation and distribution of eclogite facies rocks in the Alps. In: Carswell DA (ed) Eclogite facies rocks. Blackie, London, pp 204–224

Enami M, Zang Q, Yin Y (1993) High-pressure eclogites in northern Jiangsu–southern Shangdong province, eastern China. J Metamorph Geol 11:589–603

Ernst WG, Liou JG (1995) Contrasting plate-tectonic styles of the Qinling–Dabie–Sulu and Franciscan metamorphic belts. Geology 23:353–356

Griffin WL, O'Reilly SY, Pearson NJ (1990) Eclogite stability near the crust-mantle boundary. In: Carswell DA (ed) Eclogite facies rocks. Blackie, London, pp 291–314

Heinrich CA (1982) Kyanite–eclogite to amphibolite facies evolution of hydrous mafic and pelitic rocks, Adula nappe, Central Alps. Contrib Mineral Petrol 81:30–38

Heinrich CA (1986) Eclogite facies regional metamorphism of hydrous mafic rocks in the central alpine Adula Nappe. J Petrol 27:123–154

Hermann J (2002) Experimental constraints on phase relations in subducted continental crust. Contrib Mineral Petrol 143:219–235

Hirajima T, Nakamura D (2003) The most representative UHP metamorphic units in the world: 2.4. The Dabie Shan–Sulu orogen. In: Carswell DA, Compagnoni R (eds) 5th EMU School and Symposium and ERASMUS IP on Ultra-high Pressure Metamorphism; a Substantial Volume of the EMU Notes in Mineralogy series. (in press)

Hirajima T, Banno S, Hiroi Y, Ohta Y (1988) Phase petrology of eclogites and related rocks from the Motalafjella high-pressure metamorphic complex in Spitsbergen (Arctic Ocean) and its significance. Lithos 22:75–97

Hirajima T, Ishiwatari A, Cong B, Zhang R, Banno S, Nozaka T (1990) Coesite from Mengzhong eclogite at Donghai county, northeastern Jiangsu province, China. Mineral Mag 54:579–583

Hirajima T, Zhang R, Li J, Cong B (1992) Petrology of the nyböite-bearing eclogite in the Donghai area, Jiangsu Province, eastern China. Mineral Mag 56:37–46

Holland TJB (1979) High water activities in the generation of high pressure kyanite eclogites of the Tauern Window, Austria. J Geol 87:1–27

Holland TJB, Powell R (1998) An internally consistent thermodynamic data set for phases of petrological interest. J Metamorph Geol 16:309–343

Ikeda T (1990) Ti endmember composition of biotite: Ti substitution in biotite from Ryoke metamorphic rocks in the Yanai district (in Japanese with English abstract). J Mineral Petrol Econ Geol 85:357–363

Izadyar J, Hirajima T, Nakamura D (2000) Talc–phengite–albite assemblage in piemontite–quartz schist of the Sanbagawa metamorphic belt, central Shikoku, Japan. Island Arc 9:145–158

Jahn B (1998) Geochemical and isotopic characteristics of UHP eclogites and ultramafic rocks of the Dabie orogen: implications for continental subduction and collisional tectonics. In: Hacker BR, Liou JG (eds) When continents collide: geodynamics and geochemistry of ultrahigh-pressure rocks. Kluwer, Dordrecht, pp 203–239

Jamtveit B (1987a) Metamorphic evolution of the Eiksunddal eclogite complex, western Norway, and some tectonic implications. Contrib Mineral Petrol 95:82–99

Jamtveit B (1987b) Magmatic and metamorphic controls on chemical variations within the Eiksunddal eclogite complex, Sunnmøre, western Norway. Lithos 20:369–389

Kienast JR, Lombardo B, Biino G, Pinardon JL (1991) Petrology of very-high-pressure eclogitic rocks from the Brossasco–Isasca Complex, Dora-Maira Massif, Italian Western Alps. J Metamorph Geol 9:19–34

Kretz R (1983) Symbols for rock-forming minerals. Am Mineral 68:277–279

Krogh EJ (1977) Evidence of Precambrian continent–continent collision in Western Norway. Nature 267:17–19

Krogh EJ (1980) Compatible P–T conditions for eclogites and surrounding gneiss in the Kristiansund areas, Western Norway. Contrib Mineral Petrol 75:387–393

Lappin MA, Smith DC (1978) Mantle-equilibrated orthopyroxene eclogite pods from the basal gneisses in the Selje District, Western Norway. J Petrol 19:530–584

Li S, Xiao Y, Liou D, Chen Y, Ge N, Zhang Z, Sun S, Cong B, Zhang R, Hart SR, Wang S (1993) Collision of the North China and Yangtse blocks and formation of coesite-bearing eclogites: timing and processes. Chem Geol 109:89–111

Liu J, Bohlen SR, Ernst WG (1996) Stability of hydrous phases in subducting oceanic crust. Earth Planet Sci Lett 143:161–171

Medaris G, Jelínek JM, Mísar Z (1995) Czech eclogites: terrane settings and implications for Variscan tectonic evolution of the Bohemian Massif. Eur J Mineral 7:7–28

Mørk MBE (1985) A gabbro to eclogite transition on Flemsøy, Sunnmøre, western Norway. Chem Geol 50:283–310

Nakamura D (1997) Pressure–temperature history and the exhumation process of ultrahigh pressure metamorphic rocks. PhD Thesis, Kyoto University, Japan

Nakamura D, Banno S (1997) Thermodynamic modelling of sodic pyroxene solid-solution and its application in a garnet–omphacite–kyanite–coesite geothermobarometer to UHP metamorphic rocks. Contrib Mineral Petrol 130:93–102

Nakamura D, Hirajima T (2000) Granulite-facies overprinting of ultrahigh-pressure metamorphic rocks, northeastern Su-Lu region, eastern China. J Petrol 41:563–583

O'Brien PJ (1993) Partially retrograded eclogites of the Münchberg Massif, Germany: records of a multi-stage Variscan uplift history in the Bohemian Massif. J Metamorph Geol 11:241–260

O'Brien PJ, Carswell DA, Gebauer D (1990) Eclogite formation and distribution in the European Variscides. In: Carswell DA (ed) Eclogite facies rocks. Blackie, London, pp 204–224

Okay AI (1995) Paragonite eclogites from Dabie Shan, China: re-equilibration during exhumation? J Metamorph Geol 13:449–460

Okrusch M, Matthes S, Klemd R, O'Brien PJ, Schmidt K (1991) Eclogites at the north-western margin of the Bohemian Massif: A review. Eur J Mineral 3:707–730

Ono S (1998) Stability limits of hydrous minerals in sediment and mid-ocean ridge basalt compositions: implications for water transport in subduction zones. J Geophys Res 103:18253–18267

Poli S, Schmidt MW (1995) H_2O transport and release in subduction zones: experimental constraints on basaltic and andesitic systems. J Geophys Res 100:22299–22314

Schmädicke E, Okrusch M, Schmidt W (1992) Eclogite-facies rocks in the Saxonian Erzgebirge, Germany: high pressure metamorphism under contrasting P–T conditions. Contrib Mineral Petrol 110:226–241

Schmidt MW (1996) Experimental constraints on recycling of potassium from subducted oceanic crust. Science 272:1927–1930

Schmidt MW, Poli S (1998) Experimentally based water budgets for dehydrating slabs and consequences for arc magma generation. Earth Planet Sci Lett 163:361–379

Simon G, Chopin C (2001) Enstatite–sapphirine crack-related assemblages in ultrahigh-pressure pyrope megablasts, Dora-Maira massif, western Alps. Contrib Mineral Petrol 140:422–440

Smith DC (1984) Coesite in clinopyroxene in the Caledonides and its implications for geodynamics. Nature 310:641–644

Smith DC (1988) A review of the peculiar mineralogy of the 'Norwegian coesite–eclogite province', with crystal-chemical, petrological, geochemical and geodynamical notes and an extensive bibliography. In: Smith DC (ed) Eclogites and eclogite-facies rocks. Elsevier, Amsterdam

Takahashi E (1986) Melting of a dry peridotite KLB-1 up to 14 GPa: implications on the origin of peridotitic upper mantle. J Geophys Res 91:9367–9382

Wain A (1997) New evidence for coesite in eclogite and gneisses: defining an ultrahigh-pressure province in the Western Gneiss region of Norway. Geology 25:927–930

Wain A, Waters D, Jephcoat A, Olijynk H (2000) The high-pressure to ultrahigh-pressure eclogite transition in the Western Gneiss Region, Norway. Eur J Mineral 12:667–687

Ye K, Cong B (1994) A possible ultrahigh pressure metamorphic layered gabbro body in Rongcheng County, Shandong Peninsular of eastern China. In: Wang J (ed) Annual report of the laboratory of lithosphere tectonic evolution. Seismological Press, Beijing, pp 119–128

Ye K, Liou J, Yao Y, Cong B, Wang Q (2001) Dehydration melting of phengite during early stage exhumation of coesite eclogites from the Sulu ultrahigh-pressure terrane, eastern China. Abstract of 6th International Eclogite Conference 179

Zhang RY, Liou JG (1997) Partial transformation of gabbro to coesite-bearing eclogite from Yangkou, the Sulu terrane, eastern China. J Metamorph Geol 15:183–202

Zhang RY, Liou JG, Cong B (1994) Petrogenesis of garnet-bearing ultramafic rocks and associated eclogites in the Su-Lu ultrahigh-P metamorphic terrane, eastern China. J Metamorph Geol 12:169–186

Zhang RY, Hirajima T, Banno S, Cong B, Liou JG (1995a) Petrology of ultrahigh-pressure rocks from the southern Su-Lu region, eastern China. J Metamorph Geol 13:659–675

Zhang RY, Liou JG, Cong B (1995b) Talc-, magnesite- and Ti-clinohumite-bearing ultrahigh-pressure meta-mafic and ultramafic complex in the Dabie Mountains, China. J Petrol 36:1011–1037

Zhang Z, Xu Z, Xu H (2000) Petrology of ultrahigh-pressure eclogites from the ZK703 drillhole in the Donghai, eastern China. Lithos 52:35–50